Mechanistic Studies of (Porphinato)Iron-Catalyzed Isobutane Oxidation. Comparative Studies of Three Classes of Electron-Deficient Porphyrin Catalysts

Kevin T. Moore,[†] István T. Horváth,*[,‡] and Michael J. Therien*[,†]

Department of Chemistry, University of Pennsylvania, Philadelphia, Pennsylvania 19104-6323, and Corporate Research Laboratories, Exxon Research and Engineering Company, Annandale, New Jersey 08801

Received March 13, 2000

We report herein a comprehensive study of (porphinato)iron [PFe]-catalyzed isobutane oxidation in which molecular oxygen is utilized as the sole oxidant; these catalytic reactions were carried out and monitored in both autoclave reactors and sapphire NMR tubes. In situ ^{19}F and ^{13}C NMR experiments, coupled with GC analyses and optical spectra obtained from the autoclave reactions have enabled the identification of the predominant porphyrinic species present during PFe-catalyzed oxidation of isobutane. Electron-deficient PFe catalysts based on 5,10,15,-20-tetrakis(pentafluorophenyl)porphyrin [$(C_6F_5)_4PH_2$], 2,3,7,8,12,13,17,18-octabromo-5,10,15,20-tetrakis(pentafluorophenyl)porphyrin [$Br_8(C_6F_5)_4PH_2$], and 5,10,15,20-tetrakis(heptafluoropropyl)porphyrin [$(C_3F_7)_4PH_2$] macrocycles were examined. The nature and distribution of hydrocarbon oxidation products show that an autoxidation reaction pathway dominates the reaction kinetics, consistent with a radical chain process. For each catalytic system examined, PFe^{II} species were shown not to be stable under moderate O_2 pressure at 80 °C; in every case, the PFe^{II} catalyst precursor was converted quantitatively to high-spin PFe^{III} complexes prior to the observation of any hydrocarbon oxidation products. Once catalytic isobutane oxidation is initiated, all reactions are marked by concomitant decomposition of the porphyrin-based catalyst. In situ ^{17}O NMR spectroscopic studies confirm the incorporation of ^{17}O from labeled water into the oxidation products, implicating the involvement of PFe−OH in the catalytic cycle. Importantly, $Br_8(C_6F_5)_4PFe$-based catalysts, which lack macrocycle C−H bonds, do not exhibit augmented stability with respect to analogous catalysts based on $(C_6F_5)_4PFe$ and $(C_3F_7)_4PFe$ species. The data presented are consistent with a hydrocarbon oxidation process in which PFe complexes play dual roles of radical chain initiator, and the species responsible for the catalytic decomposition of organic peroxides. This modified Haber−Weiss reaction scheme provides for the decomposition of *tert*-butyl hydroperoxide intermediates via reaction with PFe−OH complexes; the PFe^{III} species responsible for hydroperoxide decomposition are regenerated by reaction of PFe^{II} with dioxygen under these experimental conditions.

Introduction and Background

The development of selective catalytic hydrocarbon oxidation reactions is of primary importance for the functionalization of natural products, drug design, development of new chemical feedstocks, and small molecule activation. The catalytic paradigm for such selective substrate oxygenations at ambient temperature has been the enzyme cytochrome P_{450} (Scheme 1).[1] While an attractive target for biomimetic catalyst development, two major problems circumvent technological application of such yet-to-be realized catalysts that derive their oxidizing equivalents from dioxygen, the world's most abundant and least-expensive oxidant: (i) the need for coreductants and (ii) the fact that one oxygen atom of O_2 is wasted in the evolution of water. These two facts highlight the quandaries for (porphinato)-iron [PFe] catalysts that are modeled after cytochrome P_{450}. For instance, in addition to adding cost to any hydroxylated or epoxidized hydrocarbons obtained by such a catalytic cycle, coreductants must be sheltered from high-valent iron oxo species responsible for selective hydrocarbon oxidation (a $P^{\bullet+}Fe^{IV}{=}O$ state, commonly referred to as compound I), yet must be available to facilitate the **2** → **3** and **4** → **6** reductive conversions outlined in Scheme 1. Such formidable requirements for an abiological catalytic system were recognized by Groves,[2−7] Traylor,[8−11] Bruice,[12−19] Meunier,[20−22] Mansuy,[23−29] Collman,[30−34]

* To whom correspondence should be addressed.
[†] University of Pennsylvania.
[‡] Exxon Research and Engineering Company. Present address: Department of Organic Chemistry, Eotvos Lorand University, Pazmany Peter Setany 1/A, H-1117 Budapest, Hungary.

(1) Dawson, J. H. *Science* **1988**, *240*, 433−439.
(2) Groves, J. T., Adhyam, D. V. *J. Am. Chem. Soc.* **1984**, *106*, 2177−2181.
(3) Groves, J. T.; Quinn, R. *Inorg. Chem.* **1984**, *23*, 3844−3846.
(4) Groves, J. T. *J. Chem. Educ.* **1985**, *62*, 928−931.
(5) Groves, J. T.; Watanabe, Y. *J. Am. Chem. Soc.* **1986**, *108*, 507−508.
(6) Groves, J. T.; Watanabe, Y. *J. Am. Chem. Soc.* **1986**, *108*, 7834−7836.
(7) Groves, J. T.; Watanabe, Y. *J. Am. Chem. Soc.* **1988**, *110*, 8443−8452.
(8) Traylor, T. G.; Marsters, J. C., Jr.; Nakano, T.; Dunlap, B. E. *J. Am. Chem. Soc.* **1985**, *107*, 5537−5539.
(9) Traylor, T. G.; Tsuchiya, S. *Inorg. Chem.* **1987**, *26*, 1338−1339.
(10) Traylor, T. G.; Miksztal, A. R. *J. Am. Chem. Soc.* **1987**, *109*, 2770−2774.
(11) Traylor, T. G.; Hill, K. W.; Fann, W. P.; Tsuchiya, S.; Dunlap, B. E. *J. Am. Chem. Soc.* **1992**, *114*, 1308−1312.
(12) Nee, M. W.; Bruice, T. C. *J. Am. Chem. Soc.* **1982**, *104*, 6123−6125.
(13) Calderwood, T. S.; Bruice, T. C. *J. Am. Chem. Soc.* **1985**, *107*, 8272−8273.
(14) Dicken, C. M.; Lu, F. L.; Nee, M. W.; Bruice, T. C. *J. Am. Chem. Soc.* **1985**, *107*, 5776−5789.
(15) Lee, W. A.; Bruice, T. C. *J. Am. Chem. Soc.* **1985**, *107*, 513−514.
(16) Dicken, C. M.; Woon, T. C.; Bruice, T. C. *J. Am. Chem. Soc.* **1986**, *108*, 1636−1643.

10.1021/ic000284o CCC: $19.00
Published on Web 06/22/2000

Scheme 1. Cytochrome P_{450} Catalytic Cycles[1]

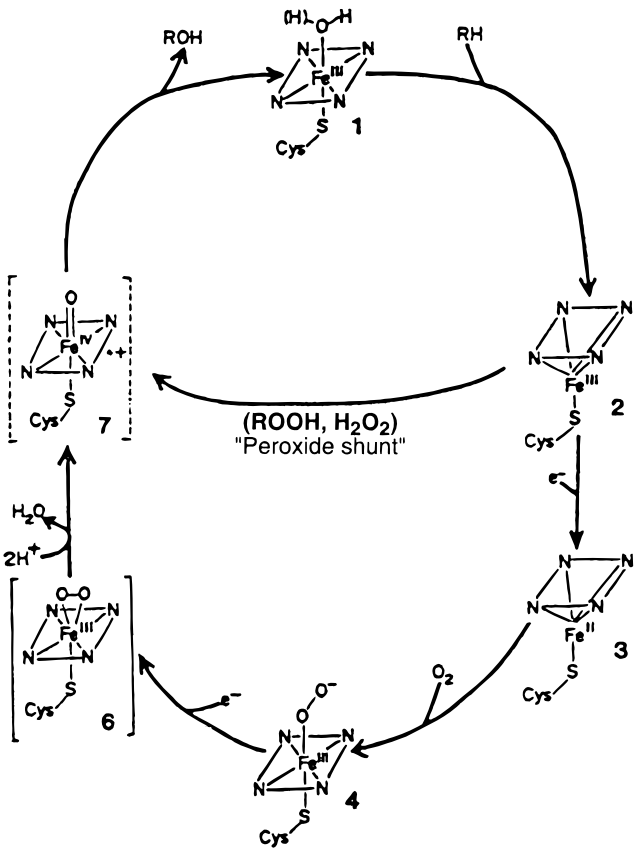

and a number of other investigators,[35−38] and have led to the development of a family of porphyrin-based P_{450}-type catalysts that utilize an abbreviated catalytic cycle (**2** → **7** → **1** → **2**) in which PFe^{III} complexes are reacted directly with powerful, sacrificial O atom donors, to produce $P^{\bullet+}Fe^{IV}$═O species that possess reactivity similar to that of compound I of cytochrome P_{450}.

Scheme 2. Proposed Mechanism for Alkane Hydroxylation Reactions Catalyzed by Electron-Deficient Iron Porphyrin Catalysts That Exploit Dioxygen as the Stoichiometric Oxidant

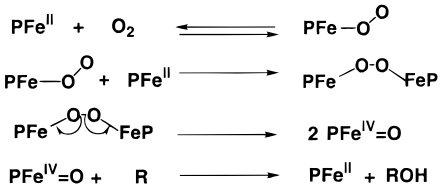

For the specialized functions of cytochrome P_{450} (detoxification, enantioselective biosynthesis of oxygenated organic substrates), Nature can afford the energetic cost to split dioxygen into water and a metal-bound O atom with the input of two protons and two electrons; most potential applications of biomimetic P_{450} catalysts cannot. For example, in a potential large-scale selective oxidation of a hydrocarbon feedstock chemical, not only would a P_{450}-type biomimetic catalyst in which one molecule of water was generated through each turn of the catalytic cycle be energetically wasteful, but the associated engineering and disposal problems would assuredly impact the economic feasibility of the process. The tremendous need for liquefied oxygenated fuels from lightweight hydrocarbons has led to a number of notions to circumvent this problem; perhaps the most intriguing hypothesis, first proposed by Ellis and Lyons,[39−47] involved the efficacy of potential electron-deficient porphyrin-based catalysts in which an Fe^{II}-derived PFe^{IV}═O species mirrors the reactivity of compound I's $P^{\bullet+}Fe^{IV}$═O oxidation level. The primary advantage of such a scheme is that both O atoms of O_2 could be incorporated into hydrocarbon substrates (Scheme 2).

Previous work showed that PFe catalysts that featured large numbers of electron-withdrawing groups fused to the macrocycle periphery facilitated the oxidation of branched hydrocarbons (particularly isobutane) to oxidized alkanes when dioxygen was utilized as the stoichiometric oxidant, suggesting that an oxidation pathway similar to that outlined in Scheme 2 might be operative.[39−47] Not only did key questions arise related to mechanism, but this work gave rise to speculation that perhaps even more electron-deficient porphyrin macrocycles could lead to the development of catalysts capable of hydroxylating primary alkanes. Work by Labinger and Gray concluded that the likely mechanism of these isobutane oxygenations was radical chain autoxidation,[48−50] where ferric and ferrous porphyrin complexes played key roles in alkyl hydroperoxide decomposition; such a

(17) Woon, T. C.; Shirazi, A.; Bruice, T. C. *Inorg. Chem.* **1986**, *25*, 5, 3845−3846.
(18) Woon, T. C.; Dicken, C. M.; Bruice, T. C. *J. Am. Chem. Soc.* **1986**, *108*, 7990−7995.
(19) Castellino, A. J.; Bruice, T. C. *J. Am. Chem. Soc.* **1988**, *110*, 158−162.
(20) Hoffmann, P.; Labat, G.; Robert, A.; Meunier, B. *Tetrahedron Lett* **1990**, *31*, 1991−1994.
(21) Hoffmann, P.; Robert, A.; Meunier, B. *Bull. Soc. Chim. Fr.* **1992**, *129*, 85−97.
(22) Hoffmann, P.; Meunier, B. *New J. Chem.* **1992**, *16*, 559−561.
(23) Mansuy, D.; Devocelle, L.; Artaud, I.; Battioni, J. P. *Nouv. J. Chim.* **1985**, *9*, 711−716.
(24) Mansuy, D. *Pure Appl. Chem.* **1987**, *59*, 759−770.
(25) Artaud, I.; Gregoire, N.; Battioni, J. P.; Dupre, D.; Mansuy, D. *J. Am. Chem. Soc.* **1988**, *110*, 8714−8716.
(26) Bartoli, J. F.; Brigaud, O.; Battioni, P.; Mansuy, D. *J. Chem. Soc., Chem. Commun.* **1991**, 440−442.
(27) Mandon, D.; Ochsenbein, P.; Fischer, J.; Weiss, R.; Jayaraj, K.; Austin, R. N.; Gold, A.; White, P. S.; Brigaud, O.; Battioni, P.; Mansuy, D. *Inorg. Chem.* **1992**, *31*, 2044−2049.
(28) Mansuy, D. *Coord. Chem. Rev.* **1993**, *125*, 129−142.
(29) Mansuy, D.; Battioni, P.; Sheldon, R. A. *Metalloporphyrins Catal. Oxid.* **1994**, 99−132.
(30) Collman, J. P.; Sorrell, T. N.; Hoffman, B. M. *J. Am. Chem. Soc.* **1975**, *97*, 913−914.
(31) Kodadek, T.; Raybuck, S. A.; Collman, J. P.; Brauman, J. I., Papazian, L. M. *J. Am. Chem. Soc.* **1985**, *107*, 4343−4345.
(32) Collman, J. P.; Hampton, P. D.; Brauman, J. T. *J. Am. Chem. Soc.* **1990**, *112*, 2977−2986.
(33) Collman, J. P.; Zhang, X.; Lee, V. J.; Uffelman, E. S.; Brauman, J. I. *Science* **1993**, *261*, 1404−1411.
(34) Collman, J. P. *Inorg. Chem.* **1997**, *36*, 5145−5155.
(35) Nappa, M. J.; Tolman, C. A. *Inorg. Chem.* **1985**, *24*, 4711−4719.
(36) Naruta, Y.; Tani, F.; Ishihara, N.; Maruyama, K. *J. Am. Chem. Soc.* **1991**, *113*, 6865−6872.
(37) Lee, K. A.; Nam, W. *J. Am. Chem. Soc.* **1997**, *119*, 1916−1922.
(38) Urano, Y.; Higuchi, T.; Hirobe, M.; Nagano, T. *J. Am. Chem. Soc.* **1997**, *119*, 12008−12009.
(39) Bhinde, M. V.; Lyons, J. E.; Ellis, P. E., Jr. U.S. Patent 5550301 A, 1996.
(40) Ellis, P. E., Jr.; Lyons, J. E. *J. Chem. Soc., Chem. Commun.* **1989**, 1189−1190.
(41) Ellis, P. E., Jr.; Lyons, J. E. *Catal. Lett.* **1989**, *3*, 389−397.
(42) Ellis, P. E., Jr.; Lyons, J. E. *J. Chem. Soc., Chem. Commun.* **1989**, 1315−1316.
(43) Ellis, P. E., Jr.; Lyons, J. E. *J. Chem. Soc., Chem. Commun.* **1989**, 1187−1188.
(44) Lyons, J. E.; Ellis, P. E., Jr. *Catal. Lett.* **1991**, *8*, 45−51.
(45) Ellis, P. E.; Jr., Lyons, J. E. *Coord. Chem. Rev.* **1990**, *105*, 181−193.
(46) Lyons, J. E.; Ellis, P. E., Jr.; Myers, H. K., Jr.; Wagner, R. W. *J. Catal.* **1993**, *141*, 311−315.
(47) Wijesekera, T. P.; Lyons, J. E.; Ellis, P. E., Jr. *Catal. Lett.* **1995**, *36*, 69−73.

mechanism accounted for the observation that primary C−H bonds were inert to functionalization under these reaction conditions.

To provide new insight into this mechanistic controversy, we brought to bear two types of in situ spectroscopy to probe the kinetics of these reactions and to examine the nature of products, reactants, and PFe species present throughout the oxidation reaction. This work couples in situ NMR spectroscopic experiments[51] with electronic absorption spectroscopic analysis of oxidation reactions carried out in autoclave reactors; such studies provide information distinct from that obtained previously from product analysis of the oxygenated hydrocarbons derived from reactions of hydrocarbons with dioxygen in the presence of PFe catalysts.

In this paper, we examine the extent to which catalyst electronic structure impacts catalyst stability and reactivity, as well as product distribution, in the catalytic oxygenation of isobutane, probing three different electron-deficient porphyrin ligand environments: 5,10,15,20-tetrakis(pentafluorophenyl)-porphyrin [$(C_6F_5)_4PH_2$], 2,3,7,8,12,13,17,18-octabromo-5,10,-15,20-tetrakis(pentafluorophenyl)porphyrin [$Br_8(C_6F_5)_4PH_2$], and 5,10,15,20-tetrakis(heptafluoropropyl)porphyrin [$(C_3F_7)_4PH_2$]. We present evidence for a radical chain autoxidation mechanism, in which (porphinato)iron(III)−OH (PFe−OH) species not only are responsible for the breakdown of the *tert*-butyl hydroperoxides generated in situ during the catalytic reaction, but also play the role of radical chain initiator in the autoxidation process.

Experimental Section

Materials. Inert atmosphere manipulations and solvent purification were carried out as described previously.[52] Methods detailing the preparation of 2,3,7,8,12,13,17,18-octabromo-5,10,15,20-tetrakis(pentafluorophenyl)porphyrin,[27] 5,10,15,20-tetrakis(pentafluorophenyl)porphyrin,[53] and 5,10,15,20-tetrakis(heptafluoropropyl)porphyrin[54] have been described previously. The syntheses of 2,3,7,8,12,13,17,18-octabromo[5,10,15,20-tetrakis(pentafluorophenyl)porphinato]iron(III) chloride and [5,10,15,20-tetrakis(pentafluorophenyl)porphinato]iron(III) chloride followed those described in the literature.[27,53,55] The syntheses of [5,10,15,20-tetrakis(heptafluoropropyl)porphinato]iron(II)−(pyridine)$_2$, and {[5,10,15,20-tetrakis(heptafluoropropyl)porphinato]iron-(III)}$_2$O have been reported recently;[56] [2,3,7,8,12,13,17,18-octabromo-5,10,15,20-tetrakis(pentafluorophenyl)porphinato]iron(II)−(pyridine)$_2$ and [5,10,15,20-tetrakis(pentafluorophenyl)porphinato]iron(II)−(pyridine)$_2$ were synthesized using an experimental procedure similar to that described for [5,10,15,20-tetrakis(heptafluoropropyl)porphinato]iron-(II)−(pyridine)$_2$.[56] Chemical shifts for ^{1}H NMR spectra are relative to residual protium in the deuterated solvents (C_6D_6, $\delta = 7.15$ ppm), while ^{19}F NMR chemical shifts are reported relative to fluorotrichloromethane ($CFCl_3$, $\delta = 0.00$ ppm). Chromatographic purification of these compounds was accomplished on the benchtop using neutral alumina (Fisher Scientific, Brockmann Activity I, 200 mesh). Elemental analyses were performed by Robertson Microlit Laboratories, Inc. (Madison, NJ). Mass spectra were performed at the Mass Spectrometry Center at the University of Pennsylvania.

General Procedure for the Preparation of (Porphinato)iron(II)−(3-Fluoropyridine)$_2$ Derivatives. The appropriate PFe−(py)$_2$ species (∼0.1 mmol) was dissolved in 3-fluoropyridine (3-F-py) (3 mL, 35.0 mmol) and brought to reflux under a N_2 atmosphere in a 50 mL Schlenk flask equipped with a condenser for 3 h. The solvent was evaporated in vacuo, and the crude PFe−(3-F-py)$_2$ complex was purified by recrystallization from hot hexanes.

[5,10,15,20-Tetrakis(heptafluoropropyl)porphinato]iron(II)−(3-F-py)$_2$. Isolated yield: 95 mg (95% based on 100 mg of $(C_3F_7)_4$PFe−(py)$_2$). ^{19}F NMR (400 MHz, C_6D_6, 20 °C): δ −79.61 (s, 12F), −84.69 (br, 8F), −118.66 (br s, 8F), −125.28 (s, 2F). UV−vis (C_6H_6) [λ_{max} (nm) (ϵ (M^{-1} cm^{-1}))]: 340 (4.47), 418 (4.95), 542 (3.76), 575 (4.28).

[5,10,15,20-Tetrakis(pentafluorophenyl)porphinato]iron(II)−(3-F-py)$_2$. Isolated yield: 95 mg (95% based on 100 mg of $(C_6F_5)_4$PFe−(py)$_2$). ^{19}F NMR (400 MHz, C_6D_6, 20 °C): δ −125.95 (s, 2F), −138.14 (s, 8F), −152.15 (t, 4F), −162.15 (d, 8F). UV−vis (C_6H_6) [λ_{max} (nm) (ϵ (M^{-1} cm^{-1}))]: 312 (4.39), 416 (5.26), 524 (4.07), 553 (3.75).

[2,3,7,8,12,13,17,18-Octabromo[5,10,15,20-tetrakis(pentafluorophenyl)porphinato]]iron(II)−(3-F-py)$_2$. Isolated yield: 95 mg (95% based on 100 mg of $Br_8(C_6F_5)_4$PFe−(py)$_2$). ^{19}F NMR (400 MHz, C_6D_6, 25 °C): δ −123.97 (s, 2F), −138.77 (s, 8F), −151.27 (t, 8F), −162.78 (d, 2F). UV−vis (C_6H_6) [λ_{max} (nm) (ϵ (M^{-1} cm^{-1}))]: 345 (4.40), 452 (5.12), 556 (3.70), 588 (3.74).

Synthesis of Four-Coordinate $(C_3F_7)_4$PFe. ZnHg amalgam was prepared using a procedure described previously by Scheidt.[57] Activated Zn turnings (600 mg, 9.23 mmol) were added to ∼ 2 mL of freshly distilled Hg, and the mixture was stirred under a N_2 atmosphere for 1 h. $(C_3F_7)_4$PFe−Cl (15 mg, 0.014 mmol) was dissolved in 2.0 mL of dry, degassed C_6D_6 and transferred to the ZnHg suspension. The mixture was stirred for 30 min, at which time the color of the solution changed from deep purple to dark green. The solution was filtered under N_2 and transferred to an NMR tube fitted with a Teflon valve. ^{1}H NMR (200 MHz, C_6D_6, 23 °C): δ −2.80 (s, 8 H). ^{19}F NMR (200 MHz, C_6D_6, 23 °C): δ −76.84 (s, 12 F); −87.57 (s, 8 F); −106.98 (br s, 8 F).

Instrumentation. Electronic spectra were recorded on an OLIS UV−vis−near-IR spectrophotometry system that is based on the optics of a Carey 14 spectrophotometer. Variable-temperature and in situ high-pressure NMR spectra were recorded on a Varian 400 MHz spectrophotometer. High-pressure NMR experiments were performed using single-crystal sapphire NMR tubes; their design has been described elsewhere.[58] GC analyses of our catalytic oxidation reactions were accomplished using a Perkin-Elmer gas chromatographic autosystem equipped with a 30 mm × 0.53 mm × 2.65 μm thickness Hewlett-Packard HP1 cross-linked methyl silicone column. A 125 mL Parr reactor equipped with a magnetic stirrer was used for the autoclave oxidations.

Autoclave Reactor Oxidation Studies. A 125 mL autoclave reaction vessel, lined with a glass sleeve, was charged with 20 mL of a 0.25 mM solution of the PFe catalyst in the appropriate solvent and a known amount of isobutane. The vessel was then heated to 80 °C, and once the temperature had equilibrated, oxygen (120 psi) was introduced into the system. An oxygen gas feed vessel was utilized to maintain constant pressure in the reactor throughout the course of the catalytic oxidation. Aliquots (2 mL) were removed periodically from the autoclave reactor for analysis; electronic absorption spectroscopy (25 °C) determined the nature of the PFe species present as a function of time, while GC experiments enabled identification and quantification of the organic products generated in the reaction. The reaction was terminated when dioxygen ceased to be consumed. After depressurization and thorough cleaning of the autoclave, the vessel was charged with solvent, isobutane, and oxygen and heated to 80 °C for 24 h to confirm that no substrate oxidation took place in the absence of catalyst. If trace catalytic activity due to reactor impurities was observed, the reactor was repetitively recleaned and retested with the catalyst-free (blank) system

(48) Grinstaff, M. W.; Hill, M. G.; Labinger, J. A.; Gray, H. B. *Science* **1994**, *264*, 1311−1313.
(49) Labinger, J. A. *Catal. Lett.* **1994**, *26*, 95−99.
(50) Boettcher, A.; Birnbaum, E. R.; Day, M. W.; Gray, H. B.; Grinstaff, M. W.; Labinger, J. A. *J. Mol. Catal., A* **1997**, *117*, 229−242.
(51) Moore, K. T.; Horváth, I. T.; Therien, M. J. *J. Am. Chem. Soc.* **1997**, *119*, 1791−1792.
(52) DiMagno, S. G.; Lin, V. S.-Y.; Therien, M. J. *J. Org. Chem.* **1993**, *58*, 5983−5993.
(53) Adler, A. D.; Longo, F. R.; Finarelli, J. D.; Goldmacher, J.; Assour, J.; Korsakoff, J. *J. Org. Chem.* **1967**, *32*, 476.
(54) DiMagno, S. G.; Williams, R. A.; Therien, M. J. *J. Org. Chem.* **1994**, *59*, 6943−6948.
(55) Birnbaum, E. R.; Hodge, J. A.; Grinstaff, M. W.; Schaefer, W. P.; Henling, L.; Labinger, J. A.; Bercaw, J. E.; Gray, H. B. *Inorg. Chem.* **1995**, *34*, 3625−3632.
(56) Moore, K. T.; Fletcher, J. T.; Therien, M. J. *J. Am. Chem. Soc.* **1999**, *121*, 5196−5209.
(57) Safo, M. K.; Nesset, M. J. M.; Walker, F. A.; Debrunner, P. G.; Scheidt, W. R. *J. Am. Chem. Soc.* **1997**, *119*, 9438−9448.
(58) Horváth, I. T.; Ponce, E. C. *Rev. Sci. Instrum.* **1991**, *62*, 1104−1105.

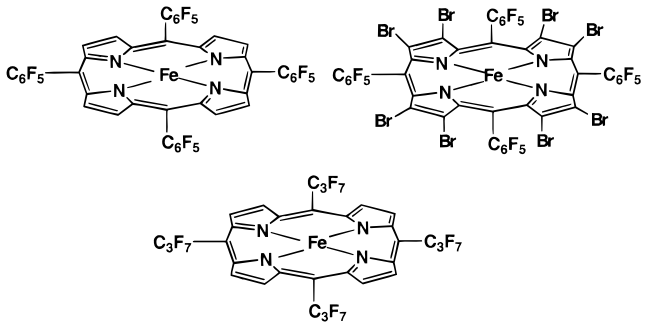

Figure 1. Electron-deficient (porphinato)iron structures.

until no hydrocarbon oxidation products could be observed for the control reaction.

High-Pressure NMR Studies of Catalytic Hydrocarbon Oxidation. Sapphire NMR tubes were charged with a 0.5 mM solution of the PFe catalyst in benzene-d_6 under argon in a glovebox. The tube was cooled in a liquid N_2 bath; isobutane was then condensed in the chilled vessel to give a hydrocarbon concentration of ~7 M. After the tube was warmed to room temperature, oxygen gas was added at a pressure of ~160 psi, providing an isobutane-rich system possessing an 8:1 molar ratio of isobutane/O_2. The NMR tubes were heated to 80 °C, and the fate of the PFe species was monitored by ^{19}F or ^{1}H NMR; the hydrocarbon oxidation products were conveniently analyzed by ^{13}C NMR. While these NMR tube reactions were run until catalysis ceased, all such reactions exhibited isobutane conversions that ranged from 5% to 10%, corresponding to incorporation of 40−80% of the O_2 present in hydrocarbon oxidation products.

***tert*-Butyl Hydroperoxide Decomposition Studies. (A) Electronic Absorption Spectroscopy.** Benzene solutions of the PFe catalysts (10^{-5} M) were transferred to a Schlenk-style optical cell sealed under N_2; a sufficient quantity of a 5 M decane solution of *tert*-butyl hydroperoxide was added at ambient temperature to provide a 1000− 3000-fold molar excess of this reagent with respect to the PFe complex. The fate of the porphyrin catalyst was monitored by electronic absorption spectroscopy.

(B) NMR Spectroscopy. PFe catalysts were dissolved in toluene-d_8 (concentration 10^{-2} M) and transferred to an NMR tube under an atmosphere of Ar; 1000 equiv of *tert*-butyl hydroperoxide was then added to the tube at −198 °C. The hydroperoxide decomposition reaction was monitored by ^{19}F NMR spectroscopy at −70 °C. GC data were analyzed for *tert*-butyl alcohol, acetone, and *tert*-butyl peroxide as well as other possible oxidation products.

Isotopic Labeling Studies. Benzene solutions of the PFe catalyst were treated with 5 μL of $^{17}OH_2$ (~20% enrichment) prior to pressurization with isobutane and unlabeled oxygen in sapphire NMR tubes. The NMR tubes were heated to 80 °C; ^{19}F and ^{17}O NMR spectra were taken alternately to monitor both the state of the PFe catalyst and degree of ^{17}O incorporation into the oxidation products as a function of time.

Results and Discussion

Synthesis of $(C_3F_7)_4$PFe, $(C_6F_5)_4$PFe, and $Br_8(C_6F_5)_4$PFe Complexes. The three electron-deficient PFe systems utilized in this study are displayed in Figure 1. All three macrocycles are appended with electronegative substituents which stabilize the Fe^{II} redox state in the presence of Lewis-basic axial ligands. The corresponding low-spin PFe−$(py)_2$ complexes can be synthesized by the reaction of the respective free base porphyrin (PH_2) with an Fe^{II} salt in pyridine at reflux. The resulting ferrous PFe−$(py)_2$ complexes can be subsequently purified via chromatography on neutral alumina (eluant 9:1 CH_2Cl_2/pyridine) in air and do not evince any observable oxidation to PFe^{III} species. These ferrous complexes are robust in the solid state and stable in aerated solutions at ambient temperature containing excess pyridine, but they are irreversibly oxidized to PFe^{III} complexes in noncoordinating solvents that lack a sufficient quantity of an appropriate Lewis base.

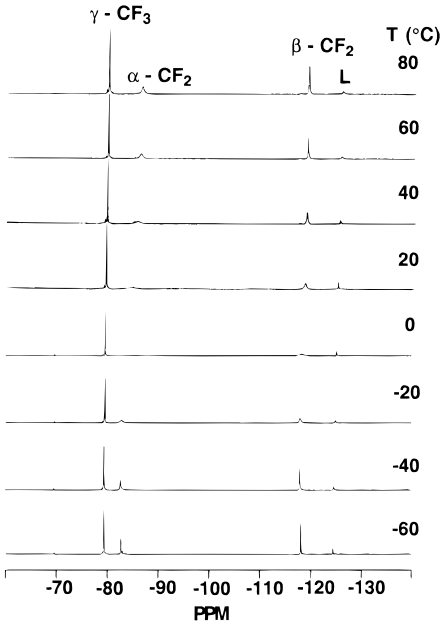

Figure 2. Variable-temperature ^{19}F NMR spectra of $(C_3F_7)_4$PFe−(3-F-py)$_2$ in toluene-d_8 under Ar. L represents the ^{19}F signal for the 3-F-py axial ligand, while α, β, and γ refer to the ^{19}F signals that derive from the *meso*-perfluoropropyl groups.

Following isolation of the PFe−$(py)_2$ complexes, facile replacement of the pyridine ligands with 3-fluoropyridine (3-F-py) was accomplished by dissolving the PFe−$(py)_2$ compound in neat 3-F-py and heating at reflux for 3 h. This axial ligand was chosen since it provides a convenient ^{19}F NMR handle for our spectroscopic studies of the catalytic isobutane oxidation reaction (vide infra). While binding constants for PFe^{III} complexes vary with the electronic properties of the axial ligands, it has been shown for conventional porphyrin macrocycles that the absolute magnitude of the analogous ligand binding constants for the corresponding PFe^{II} derivatives does not depend appreciably on the acidity constant for the BH^+/B couple of the axial Lewis base; PFe−L_2 formation constants are in fact relatively uniform for axial ligands having pK_a values that range from 0.7 to 10.1.[59]

NMR Spectroscopy. Figure 2 displays temperature-dependent ^{19}F NMR spectral data obtained for $(C_3F_7)_4$PFe−(3-F-py)$_2$ in toluene-d_8 over a −60 to +80 °C temperature domain; detailed, tabulated variable-temperature (VT) ^{19}F NMR data for $(C_3F_7)_4$PFe−(3-F-py)$_2$, $(C_6F_5)_4$PFe−(3-F-py)$_2$, and $Br_8(C_6F_5)_4$PFe−(3-F-py)$_2$ complexes are presented in the Supporting Information. For the $(C_3F_7)_4$PFe−(3-F-py)$_2$ complex, four distinct ^{19}F NMR resonances are observed; the three *meso*-heptafluoropropyl signals are denoted as α, β, and γ, while the single 3-F-py axial ligand signal is labeled as L. The temperature-dependent NMR behavior for this compound is complex. Note that the α-CF_2 and β-CF_2 resonances broaden as the sample is warmed from −60 to 0 °C, but progressively sharpen and shift to higher field upon further increases in temperature. These temperature-dependent shifts and changes in breadth of the C_3F_7 ^{19}F NMR signals derive from two factors: the magnitude of the barrier to rotation of the CF_2−C_{meso} bond as a function of coordination number, and the fact that diamagnetic [$(C_3F_7)_4$-

(59) Walker, F. A.; Nasri, H.; Turowska-Tyrk, I.; Mohanrao, K.; Watson, C. T.; Shokhirev, N. V.; Debrunner, P. G.; Scheidt, W. R. *J. Am. Chem. Soc.* **1996**, *118*, 12109−12118.

PFe−(3-F-py)$_2$] is in equilibrium in solution with paramagnetic five- and four-coordinate species. [56]

Because coordinatively unsaturated PFe^{II}−L or PFe^{II} species derived from PFe^{II}−L$_2$ catalyst precursors will be reactive with dioxygen, we examined the temperature-dependent axial ligand dynamics using VT ^{1}H NMR ((C$_3$F$_7$)$_4$PFe−(L)$_2$, (C$_6$F$_5$)$_4$PFe−(L)$_2$) and VT ^{19}F NMR ((C$_3$F$_7$)$_4$PFe−(L)$_2$, (C$_6$F$_5$)$_4$PFe−(3-F-py)$_2$, Br$_8$(C$_6$F$_5$)$_4$PFe−(3-F-py)$_2$) spectroscopies (L = 3-F-py, pyridine). While these data (presented as Supporting Information) will be analyzed in detail elsewhere, it is important to note that all of these species show spectral behavior consistent with the presence of significant concentrations of PFe species with reduced coordination number (PFe and PFe−L complexes) at 80 °C.

One interesting aspect of these data is the apparent disparate temperature-dependent axial ligand dynamical behavior that is manifest as a function of macrocycle electronic structure; (C$_3$F$_7$)$_4$PFe binds ligands more avidly than (C$_6$F$_5$)$_4$PFe and Br$_8$-(C$_6$F$_5$)$_4$PFe, consistent with axial ligand binding constant data determined from electrochemical experiments.[56] Moreover, in contrast to what has been observed for more conventional porphyrin macrocycles,[59] axial ligand binding affinity increases markedly with increasing Lewis basicity of the axial donor for (C$_3$F$_7$)$_4$PFe−(L)$_2$ species, consistent with the strongly σ-electron-withdrawing nature of the macrocycle's *meso*-perfluoroalkyl groups.[56]

To quantify the magnitude of the axial pyridyl binding constant, four-coordinate (C$_3$F$_7$)$_4$PFe was synthesized; ^{1}H NMR spectroscopy (Supporting Information) shows that the β-H atoms resonate at −2.80 ppm at 23 °C and exhibit Curie behavior, shifting to lower field with increasing temperature. Because $K_2 \gg K_1$ (eq 1) for nitrogenous PFe^{II} axial ligands,[60−62] and the

$$\text{PFe}-\text{L}_2 \overset{K_1}{\rightleftharpoons} \text{PFe}-\text{L} + \text{L} \overset{K_2}{\rightleftharpoons} \text{PFe} + 2\text{L} \qquad (1)$$

σ-electron- withdrawing nature of the (C$_3$F$_7$)PH$_2$ macrocycle engenders exceptional stability to the ferrous oxidation state when the metal resides in the macrocycle plane (thus destabilizing (C$_3$F$_7$)$_4$PFe(py) relative to both (C$_3$F$_7$)$_4$PFe(py)$_2$ and (C$_3$F$_7$)$_4$-PFe),[56] the equilibrium constant for axial pyridyl binding can be determined from this temperature-dependent NMR data, giving $K_{eq} = (3.0 \pm 0.6) \times 10^9$ for the overall formation constant (β_2) of the six-coordinate complex at 23 °C; note that an axial pyridyl binding constant of this magnitude exceeds by over a 1000-fold that determined for ferrous centers of conventional porphyrin macrocycles.[63,64]

High-Pressure NMR Spectroscopic Studies. NMR experiments that examined the spectroscopic behavior of (C$_3$F$_7$)$_4$PFe−(3-F-py)$_2$, (C$_6$F$_5$)$_4$PFe−(3-F-py)$_2$, and Br$_8$(C$_6$F$_5$)$_4$PFe−(3-F-py)$_2$ catalyst precursors under high dioxygen pressure in the presence and absence of isobutane substrate were carried out. Figures 3 and 4 detail these studies for systems utilizing (C$_3$F$_7$)$_4$PFe−(3-F-py)$_2$ and (C$_6$F$_5$)$_4$PFe−(3-F-py)$_2$ catalyst precursors. In contrast to earlier work that has emphasized the stability of Br$_8$(C$_6$F$_5$)$_4$-PFe-based oxidation catalysts,[40−45,65] under the experimental conditions explicated in this paper, these catalysts show the least

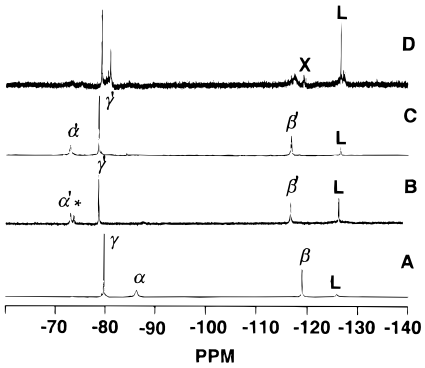

Figure 3. In situ ^{19}F NMR spectra of a PFe-catalyzed isobutane oxidation reaction in benzene-d_6 that employed (C$_3$F$_7$)$_4$PFe−(3-F-py)$_2$ as the catalyst precursor. (A) (C$_3$F$_7$)$_4$PFe−(3-F-py)$_2$ at 80 °C under Ar. (B) (C$_3$F$_7$)$_4$PFe species present 2 days after pressurization with O$_2$ in the *absence* of isobutane at 80 °C. (C) (C$_3$F$_7$)$_4$PFe species observable at 80 °C 1 h following the addition of isobutane/O$_2$. (D) (C$_3$F$_7$)$_4$PFe-derived species that are observed while oxidation products are being produced (reaction time 96 h at 80 °C, spectrum taken at 26 °C). Prime notation represents the ^{19}F NMR signals that coincide with those reported for [(C$_3$F$_7$)$_4$PFe]$_2$O.[56] L represents the ^{19}F NMR resonance for the 3-F-py axial ligand ($\delta = -127.1$ ppm), and X denotes the ^{19}F NMR signal corresponding to pyridine *N*-oxide; the signal denoted with an asterisk is tentatively assigned to (C$_3$F$_7$)$_4$PFe−OH.

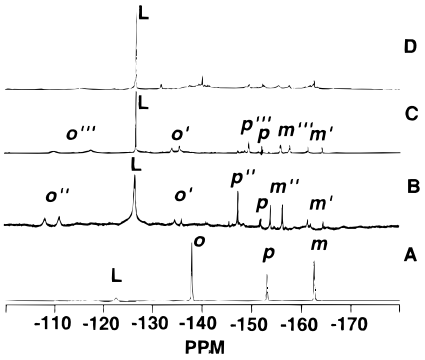

Figure 4. In situ ^{19}F NMR spectra of a (C$_6$F$_5$)$_4$PFe−(3-F-py)$_2$-catalyzed isobutane oxidation reaction in benzene-d_6. (A) (C$_6$F$_5$)$_4$PFe−(3-F-py)$_2$ at 80 °C under Ar. (B) (C$_6$F$_5$)$_4$PFe species present 2 days after pressurization with O$_2$ in the *absence* of isobutane at 80 °C. (C) (C$_6$F$_5$)$_4$-PFe species observable at 80 °C 1 h following addition of O$_2$/isobutane. (D) ^{19}F NMR spectrum taken after oxidation products are first observed (reaction time 48 h at 80 °C; spectrum taken at 26 °C). Prime notation represents the ^{19}F NMR resonances corresponding to [(C$_6$F$_5$)$_4$PFe]$_2$O. The double prime notation denotes the ^{19}F NMR signals assignable to (C$_6$F$_5$)$_4$PFe−OH. The triple prime notation denotes resonances that are tentatively ascribed to a (C$_6$F$_5$)$_4$PFe−(O-*tert*-butyl) complex. L signifies the 3-F-py axial ligand resonance.

stability, and evince (in contrast to analogous data obtained for reactions that employed (C$_3$F$_7$)$_4$PFe−(3-F-py)$_2$ and (C$_6$F$_5$)$_4$PFe−(3-F-py)$_2$ catalyst precursors) NMR signals that could not readily be ascribed to well-characterized PFe complexes. As such, detailed analyses of NMR data obtained for Br$_8$(C$_6$F$_5$)$_4$PFe-catalyzed reactions are not possible; these spectra are presented for comparative purposes in the Supporting Information.

Reactivity of (Porphinato)iron Species with Dioxygen. Sapphire NMR tubes containing the (C$_3$F$_7$)$_4$PFe−(3-F-py)$_2$ and (C$_6$F$_5$)$_4$PFe−(3-F-py)$_2$ catalyst precursors were prepared under argon, and their ^{19}F NMR spectra were recorded at 80 °C (Figures 3A and 4A). The tubes were then pressurized with dioxygen (∼160 psi); the ^{19}F NMR spectra shown in Figures

(60) Wayland, B. B.; Mehne, L. F.; Swartz, J. *J. Am. Chem. Soc.* **1978**, *100*, 2379−2383.
(61) Rougee, M., Brault, D. *Biochem. Biophys. Res. Commun.* **1973**, *55*, 1364−1369.
(62) Rougee, M.; Brault, D. *Biochemistry* **1975**, *14*, 4100−4106.
(63) Kadish, K. M.; Bottomley, L. A. *Inorg. Chem.* **1980**, *19*, 832−836.
(64) Nesset, M. J. M.; Shokhirev, N. V.; Enemark, P. D.; Jacobson, S. E.; Walker, F. A. *Inorg. Chem.* **1996**, *35*, 5188−5200.
(65) Lyons, J. E.; Ellis, P. E., Jr.; Durante, V. A. *Stud. Surf. Sci. Catal.* **1991**, *67*, 99−116.

3B and 4B were manifest immediately at 80 °C. No further spectral changes were observed over a one-week period at 80 °C. Figure 3B reveals two new distinct resonances for the α-CF_2 fluorines, one of which is assigned to $[(C_3F_7)_4PFe]_2O$ (prime notation).[56] Figure 4B shows that a mixture of PFe−OH (double prime label) and $[PFe]_2O$ (single prime label) exists for the $(C_6F_5)_4PFe$ system under dioxygen; note that multiple species are present under these conditions for the $Br_8(C_6F_5)_4PFe$ system (Supporting Information). In these NMR experiments, it is important to emphasize that, at 80 °C under the dioxygen pressure utilized, ferrous porphyrin species are not observed for any of these electron-deficient ligand environments. All three PFe−(3-F-py)$_2$ systems evince (i) complete loss of the axial ligand following O_2 pressurization, (ii) an NMR signal that integrates as 2 equiv of the free 3-F-py ligand, and (iii) the quantitative conversion to exclusively PFe^{III} species after O_2 is added, suggesting that the oxidizing agent involved in the ferrous-to-ferric conversion derives solely from dioxygen. Analogous experiments utilizing $(C_3F_7)_4PFe-(3\text{-F-py})_2$ catalyst precursor concentrations as high as 0.1 M (data not shown) reveal stoichiometric conversion to the PFe^{III} species highlighted in Figure 3B under similar O_2 pressures, effectively ruling out solvent impurities (e.g., peroxides) playing a significant role in PFe^{II} oxidation. Hence, these experiments show that while $Br_8(C_6F_5)_4PH_2$ and $(C_3F_7)_4PH_2$ similarly stabilize the ferrous oxidation state,[56] neither class of these exceptionally electron-poor PFe^{II} complexes is thermodynamically stable under moderate O_2 pressure at 80 °C.

Differences between the ^{19}F NMR spectra of Figures 3B and 4B lie in the identities and distribution of the predominant PFe^{III} species present under dioxygen; the nature of these PFe^{III} species clearly depends on the steric and electronic properties of the macrocyclic ligands. In Figure 3, we observe conversion of the ferrous porphyrin complex to $[(C_3F_7)_4PFe]_2O$ μ-oxo dimer upon O_2 pressurization, the spectral properties of which have been previously reported.[56] The resonance labeled with an asterisk in Figure 3B has not been conclusively identified; it is likely, however, that it corresponds to $(C_3F_7)_4PFe-OH$, though such a species has yet to be independently isolated and characterized. Similarly, when solutions of $(C_6F_5)_4PFe-(3\text{-F-py})_2$ are pressurized with dioxygen at 80 °C, a mixture of $[(C_6F_5)_4PFe]_2O$ and $(C_6F_5)_4PFe-OH$ species[55] exist in nearly equal proportion (Figure 4B). Due to steric factors that derive from the $Br_8(C_6F_5)_4PH_2$ macrocycle's highly saddled structure, the formation of a $[Br_8(C_6F_5)_4PFe]_2O$ μ-oxo dimer species[66] is precluded; hence, all ferric porphyrin species present when solutions of $Br_8(C_6F_5)_4PFe-(3\text{-F-py})_2$ are pressurized with dioxygen at 80 °C (Supporting Information) must correspond to mononuclear ferric complexes.

High-Pressure NMR Spectroscopic Studies of PFe-Catalyzed Isobutane Oxidation Reactions that Utilize Dioxygen. Sapphire NMR tubes were charged with benzene-d_6, a PFe−(3-F-py)$_2$ complex, isobutane, and oxygen; these tubes were then heated at 80 °C (see the Experimental Section); substrate oxidation products were monitored and quantitated by ^{13}C or ^{17}O NMR spectroscopy, while ^{19}F NMR was used to characterize the porphyrinic species present in solution. Since substrate-to-product conversions could be rate limited by O_2 transfer from the gas to solution phase across the small gas−liquid interface of the NMR tube, a more detailed analysis of the product distribution with respect to time was obtained for isobutane oxidation reactions carried out in autoclaves (vide infra). Nevertheless, these NMR experiments provide the first direct analysis of the predominant PFe species that exist when the catalytic conversion of isobutane to isobutanol commences.[51] Furthermore, they illuminate the time-dependent spectral changes that take place for these three classes of electron-deficient PFe species while isobutane is being oxidized. Concomitantly obtained ^{13}C and/or ^{17}O NMR data allow us to chronicle the time-dependent distribution of organic products, as well as determine the approximate times that the catalytic oxidation reaction initiates and ceases.

Figures 3C and 4C show the ^{19}F NMR spectral data obtained for the systems that, respectively, employ $(C_3F_7)_4PFe-(3\text{-F-py})_2$ and $(C_6F_5)_4PFe-(3\text{-F-py})_2$ catalyst precursors, once pressurization with isobutane and dioxygen has taken place. Note that Figure 4C indicates that, upon isobutane addition, the concentration of $(C_6F_5)_4PFe-OH$ has diminished, and at least one new PFe^{III} species is present. On the basis of the similarity of the chemical shifts of its resonances to those of $(C_6F_5)_4PFe-OH$, we tentatively assign this complex as a $(C_6F_5)_4PFe-(O\text{-}tert\text{-butyl})$ species. Whatever the nature of this compound, we have to date only observed it under catalytic conditions. Figures 3D and 4D reveal the PFe species observable in solution at the onset of catalysis, which we define as the point at which the first evidence of oxidation products is observable in the ^{13}C NMR spectrum. Comparison of the ^{19}F NMR data presented in panels C and D of Figures 3 and 4 with the corresponding ^{13}C NMR spectral data utilized to monitor the isobutane oxidation products (data not shown) make apparent several general trends: (i) No oxidation products are observed immediately upon tube pressurization with isobutane and dioxygen (Figures 3C and 4C); note also that only PFe^{III} species are observable at this stage in each of these three systems. (ii) In each experiment, an induction period is observed during which no further PFe spectral changes are evident in the ^{19}F NMR spectrum and no oxidation products are detectable by ^{13}C NMR spectroscopy; for Figures 3 and 4, the induction period spans the time between the acquisition of the NMR spectra C and D. (iii) For the $(C_3F_7)_4PFe$- and $(C_6F_5)_4PFe$-based catalysts**,** the length of the induction period ranges from several hours to several days; for catalytic oxidations employing $Br_8(C_6F_5)_4PFe-(3\text{-F-py})_2$ catalyst precursors, the observed induction periods are typically less than 1 h (Supporting Information). When $(C_3F_7)_4PFe$- and $(C_6F_5)_4PFe$-based catalysts are employed, the duration of the induction period increases at higher PFe concentrations; in contrast, the induction periods for $Br_8(C_6F_5)_4PFe$-catalyzed isobutane oxidations are insensitive to the concentration of the $Br_8(C_6F_5)_4PFe-(3\text{-F-py})_2$ catalyst precursor (data not shown). These experiments demonstrate that the duration of the induction period is a function of the nature of the catalyst precursor; for a given $PFe-L_2$ concentration, the length of the induction period varies with the steric properties of the PFe species $[(C_3F_7)_4PFe > (C_6F_5)_4PFe \gg Br_8(C_6F_5)_4PFe]$. Given the apparent dependence of the induction period upon the extent of steric encumbrance at the macrocycle periphery, it is thus plausible that greater concentrations of $[PFe]_2O$ relative to PFe−OH at the onset of catalysis are responsible for longer induction periods, congruent with the supposition that the $[PFe]_2O$ dimer is catalytically inert.[51]

Following the induction period, *tert*-butyl peroxide, acetone, and *tert*-butyl alcohol were observed as the dominant oxidation products for each catalyst. Once oxidation is initiated, new porphyrinic resonances are observed in the ^{19}F NMR spectra (Figures 3D and 4D; Supporting Information); these signals diminish slowly in intensity during the course of the reaction, indicating that the benzene-soluble PFe species are decomposing

(66) Grinstaff, M. W.; Hill, M. G.; Birnbaum, E. R.; Schaefer, W. P.; Labinger, J. A.; Gray, H. B. *Inorg. Chem.* **1995**, *34*, 4896−4902.

during isobutane oxidation. For all three catalyst systems, the oxidation ceases at the time when no porphyrin species could be observed by NMR; at this point in time, typically 40−80% of the O_2 present originally in the NMR tube had been consumed. Importantly, these results show clearly that even the perhalogenated dodecasubstituted porphyrin macrocycle, $Br_8(C_6F_5)_4PH_2$, is not robust under the conditions of catalytic isobutane oxidation; this is contrary to the supposition that a macrocycle void of C−H bonds would necessarily be rendered less susceptible to oxidative degradation, as well as to a number of other previous reports.[40−45,65]

Batch Reactor Studies on PFe-Catalyzed Isobutane Oxidation Reactions That Utilize Dioxygen. To compliment the in situ NMR experiments, an analogous set of isobutane oxidation reactions were performed in a glass-lined autoclave. Unlike the NMR experiments, the batch reactor studies enable detailed kinetic analyses of the catalytic isobutane oxidation reactions and, importantly, direct monitoring of dioxygen consumption throughout an autoclave reactor oxidation, which is experimentally untenable in the NMR tube reactions. Control experiments in which the autoclave reactors are charged with benzene, isobutane, and oxygen were performed to verify that no oxidation took place in the absence of a PFe complex; if any activity was observed in the control experiments, the autoclave was repetitively cleaned and retested until no detectable hydrocarbon oxidation products were observable in the catalyst-free oxidation experiment.

Typically, the reactors were charged with benzene, PFe−(3-F-py)$_2$, and isobutane and heated to 80 °C with stirring. The only reaction conditions that differed between the catalytic oxidation experiments carried out in NMR tubes and the autoclave reactors were catalyst concentration (NMR experiments, [PFe] = 0.5 mM; autoclave oxidations, [PFe] = 0.25 mM) and the fact that the reactor utilized a continuous O_2 feed that maintained constant pressure. After oxygen was introduced to the reactor, an immediate reduction in pressure in the oxygen gas feed vessel was observed, indicating the dissolution of O_2 in the reaction medium. Samples were drawn from the reactor at various time intervals and analyzed by GC and electronic absorption spectroscopy. Parts A−C of Table 1A−C show the batch reactor data for reactions charged, respectively, with $(C_3F_7)_4$PFe, $(C_6F_5)_4$PFe, and $Br_8(C_6F_5)_4$PFe catalyst precursors. Product distribution, turnover frequency, and conversion (%) were consistent with those observed in the NMR tube experiments; the observed induction periods, however, were significantly shorter in the autoclave experiments relative to those observed for the NMR tube reactions. The shorter induction periods for the autoclave reactions may derive from better mixing of O_2 with solvent in an autoclave reactor equipped with a magnetic stirrer relative to an NMR tube which was neither stirred nor spun. It should be noted that the larger concentration of the PFe catalyst in the NMR tube experiments was necessitated by the practical requirement of minimizing the acquisition time required to obtain an adequate signal-to-noise ratio.

As seen in Table 1, three primary oxidation products were obtained in the autoclave reactor studies: *tert*-butyl alcohol, acetone, and *tert*-butyl peroxide. The distribution of these oxidation products is consistent with that observed in the NMR tube experiments; importantly the observed *tert*-butyl alcohol/acetone/*tert*-butyl peroxide distribution is indicative of an autoxidation process for isobutane oxidation as discussed by Labinger and Gray.[48,50,67] Congruent with such a mechanism, the quantity and nature of isobutane oxidation products do not appear to significantly depend on porphyrin macrocycle steric and electronic properties; instead the concentration of the PFe species utilized and the nature of the solvent appear to be much more important factors. Entry 3 of Table 1B, which describes a catalytic system with a PFe concentration 20-fold greater than that of the other experiments listed therein, shows a much higher relative percentage of the *tert*-butyl peroxide oxidation product; it is also noteworthy that, at this catalyst concentration, drastically reduced turnover numbers are observed. In further agreement with a hydrocarbon autoxidation mechanism[49] is the observed dependence of the overall conversion of isobutane to products upon reaction time, which also appears independent of macrocycle electronic properties.

As would be expected from a radical process dominating PFe-catalyzed isobutane oxidation, irreproducibility from experiment to experiment is observed with respect to the length of the induction periods, turnover frequency, and product distribution. For example, Figure 5 shows a plot of turnover frequency vs reaction time for four independent $Br_8(C_6F_5)_4$PFe-catalyzed isobutane oxidation reactions carried out under identical conditions. Note that the initial turnover frequency, the rate at which this turnover frequency diminishes, and the final turnover frequency differ for each catalytic run, despite the extreme care taken to hold all controllable experimental parameters constant. Because such discrepancies exist between catalytic oxidations carried out under presumably identical conditions, little can be concluded regarding any potential roles that catalyst electronic properties (Table 1) play in these reactions.

In addition to the major oxidation products described above, there are two oxidation products characterized in gas-phase GC analyses of these reactions that are produced in measurable quantity: CO_2 and CO. It is plausible that these products derive from the methyl radical generated in the conversion of isobutyloxy radical to acetone (vide infra).

(Porphinato)iron optical absorption properties are sensitive to macrocycle electronic structure, the oxidation state of the iron center, and the number and nature of axial ligands. Figure 6A shows the time-dependent spectral changes that occur throughout an oxidation reaction carried out in an autoclave that was initially charged with $(C_3F_7)_4$PFe−$(py)_2$, benzene, and isobutane, under conditions described previously; at $t = 0$, three intense transitions are observed at 418, 542, and 578 nm ($\log \epsilon$ = 4.95, 3.76, and 4.28, respectively).[56] Consistent with NMR tube experiments, at 80 °C following pressurization with dioxygen, quantitative conversion of the PFe^{II} complex to PFe^{III} species is evident in the $t = 1$ h electronic spectrum of Figure 6A, which displays broad Soret features at 378 and 420 nm and Q-band absorbances at 560 and 602 nm; this spectrum corresponds to that previously reported for $[(C_3F_7)_4PFe]_2O$.[56] Similar to the NMR experiments discussed above, the $t = 1$ h spectrum of Figure 6A is observed as soon as an optical spectrum can be obtained after the autoclave is charged with isobutane and dioxygen ($t \approx 5$ min), indicating that the PFe^{II}-to-PFe^{III} conversion is rapid. Furthermore, as was shown in Figures 3 and 4, catalyst degradation occurs after the onset of catalytic activity; this is marked by a steady decrease in absorption oscillator strength throughout the 350 → 650 nm spectral regime during the time domain over which isobutane oxidation is observed (Figure 6A). The 2 and 20 h spectra of Figure 6A show that a $(C_3F_7)_4$PFe-derived absorbing species is present while catalytic isobutane oxidation is taking place; the fact that these spectra cannot be fit as an appropriately weighted sum of the optical spectra of independently characterized PFe^{II},

(67) Birnbaum, E. R.; Grinstaff, M. W.; Labinger, J. A.; Bercaw, J. E.; Gray, H. B. *J. Mol. Catal., A* **1995**, *104*, 119−122.

Table 1. Time-Correlated Product Distribution of $(C_3F_7)_4$PFe-, $(C_6F_5)_4$PFe-, and $Br_8(C_6F_5)_4$PFe-Catalyzed Isobutane Oxidations at 80 °C[a]

						selectivity (%)[e]		
entry	catalyst (mmol)	solvent	reaction time (h)[b]	no. of turnovers[c]	conversion[d] (%)	*tert*-butyl alcohol	acetone	*tert*-butyl peroxide
		A. $(C_3F_7)_4$PFe-Catalyzed Oxidation						
1	$(C_3F_7)_4$PFe−$(py)_2$ (0.005)	benzene	1	2034	3.38	84.2	7.0	8.8
			2	4120	6.84	83.9	7.4	8.7
			3	5422	9.15	82.3	7.2	10.5
			5	9292	16.51	76.4	7.2	16.4
			21	9974	16.98	80.5	8.0	11.5
2	$(C_3F_7)_4$PFe−$(py)_2$ (0.005)	benzene (dried over Na)	5	460	0.77	78.3	4.3	17.4
			23.5	7800	13.99	69.5	5.4	25.1
3	$(C_3F_7)_4$PFe−(3-F-py)$_2$ (0.005)	benzene	2	3010	4.99	81.0	6.0	13.0
			19	4340	7.40	78.3	5.5	16.1
			43	5720	9.87	76.9	5.6	17.5
			91	22440	35.54	84.0	8.1	7.8
4	$(C_3F_7)_4$PFe−(3-F-py)$_2$ (0.005)	C_7F_{14}	22	8340	12.33	93.3	3.6	3.1
5	$(C_3F_7)_4$PFe−(3-F-py)$_2$ (0.005)	9:1 C_7F_{14}/benzene	22	9320	13.94	90.8	5.6	3.6
6	$(C_3F_7)_4$PFe−Cl (0.005)	benzene	18	2540	3.65	91.3	7.1	1.6
			90	3440	4.92	89.5	9.3	1.2
			114	8080	11.47	90.6	8.9	0.5
7	$[(C_3F_7)_4PFe]_2O$ (0.005)	benzene	1.5	1400	2.27	90.0	2.9	7.1
			17	5200	8.52	88.5	3.5	8.1
			91	6560	11.00	85.4	4.0	10.7
		B. $(C_6F_5)_4$PFe-Catalyzed Isobutane Oxidation						
1	$(C_6F_5)_4$PFe−Cl (0.005)	benzene	1	1418	2.77	64.0	4.5	31.5
			2	1870	3.74	61.1	4.4	34.5
			4	2058	4.18	59.3	4.3	36.4
			21	2438	5.01	57.9	4.0	38.1
			28	3582	7.39	57.4	4.0	38.6
			44	3914	8.09	56.9	4.0	39.0
			121	6500	12.74	64.4	3.8	31.8
2	$(C_6F_5)_4$PFe−Cl (0.005)	20:1 benzene/water	2	6166	9.56	87.1	7.7	5.3
			5	13920	21.48	86.3	8.9	4.8
			71	21774	34.08	83.0	10.7	6.3
3	$(C_6F_5)_4$PFe−Cl (0.100)	benzene	2	0	0.00			
			20	74	2.92	55.4	4.1	40.5
			72	290	10.97	60.7	4.5	34.8
4	$(C_6F_5)_4$PFe−OH/$[(C_6F_5)_4PFe]_2O$ (0.005)[f]	benzene	5	7840	13.93	81.4	7.4	11.2
			47	10060	18.40	78.1	7.4	14.5
5	$(C_6F_5)_4$PFe−OH/$[(C_6F_5)_4PFe]_2O$ (0.005)	20:1 benzene/1.0 M aq NaOH	19	8140	13.15	82.6	4.9	12.5
			43	9340	15.42	80.1	4.9	15.0
			70	11320	18.84	79.0	5.1	15.9
			84	15100	24.90	79.9	5.3	14.8
		C. $Br_8(C_6F_5)_4$PFe-Catalyzed Isobutane Oxidation						
1	$Br_8(C_6F_5)_4$Fe−Cl (0.005)	benzene	1	1894	3.57	77.0	5.9	17.1
			3	2174	4.12	76.4	5.8	17.8
			6	2472	4.74	75.0	6.0	19.0
2	$Br_8(C_6F_5)_4$PFe−$(py)_2$ (0.005)	benzene	42	1830	3.29	71.0	1.7	27.2
			187	10640	15.02	73.6	5.0	21.4
3	theoretical result for the radical chain mechanism[g]				22	85.0	8.5	7.0

[a] All catalytic oxidations except entry 1 of part C were performed to the exhaustive limit, which we define as the point in time where PFe species are no longer observed by electronic spectroscopy and O_2 consumption is negligible for a period of 8 h. Reaction conditions are elaborated in the Experimental Section. [b] For reactions carried out to the exhaustive limit, the last reaction data point recorded per entry corresponds to the time at which the production of oxidized hydrocarbons had completely ceased. [c] Turnovers are defined as total millimoles of product per millimole catalyst. [d] Conversion (%) is defined as the total millimoles of product per millimole of isobutane times 100%. The amount of isobutane utilized in these experiments ranged from 0.46 to 0.48 mol. [e] Selectivity is based on the relative intensities of the three oxidation products *tert*-butyl alcohol, acetone, and *tert*-butyl peroxide in the GC analyses. Other oxidation products comprised <1% of the total integrated peak intensities for *tert*-butyl alcohol, acetone, and *tert*-butyl peroxide in the GC experiments. [f] PFe−OH and $(PFe)_2O$ species exist as an equilibrium mixture; at ambient temperature, in H_2O-saturated benzene, the molar ratio of these PFe complexes is approximately 1:1. [g] See ref 49.

$PFe^{II}-L_2$, $PFe^{III}-X$, $(PFe^{III})_2O$, and $PFe^{III}-L_2$ complexes strongly suggests that porphyrin macrocycle destruction occurs over the time course of this experiment; consistent with this, considerable precipitate is observed at the reaction end point, further supporting this hypothesis. Likewise, systems utilizing $(C_6F_5)_4$PFe−Cl and $Br_8(C_6F_5)_4$PFe−Cl catalyst precursors also evince prominent changes in their electronic spectral features once catalysis has initiated, along with similar diminishment of absorption intensity in the visible and low-energy UV regions of the electromagnetic spectrum (Figure 6B,C). Note that, under these autoclave reactor conditions, complete bleaching of $Br_8(C_6F_5)_4$PFe-derived electronic absorption spectral features is observed at $t = 20$ h; consistent with the results from NMR studies of the catalytic isobutane oxidation reaction, the $Br_8(C_6F_5)_4PH_2$ macrocycle is seen to be the least robust under catalytic conditions, contrasting previous reports of its superior stability with respect to oxidative degradation.[40−45,65] For the PFe-catalyzed isobutane oxidations carried out in batch reactors, it is important to note that regardless of the PFe catalyst precursor employed, cessation of catalysis coincided with the

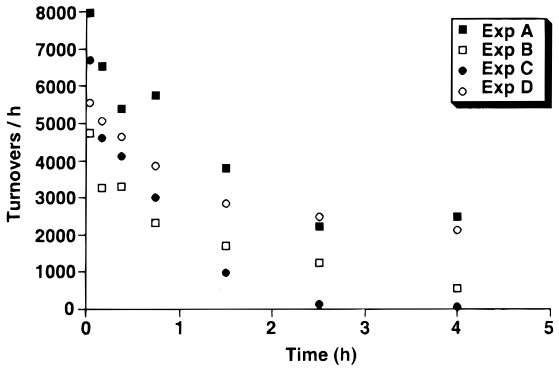

Figure 5. Turnover frequency vs reaction time for four independent $Br_8(C_6F_5)_4PFe$-catalyzed isobutane oxidations that employed identical reaction conditions ($[Br_8(C_6F_5)_4PFe] = 0.25$ mM; [isobutane] = 22.8 mM; $P_{O_2} = 8$ bar). Aliquots (2 mL) were taken out of the reaction mixture at 5, 15, 30, 60, 120, 180, and 300 min intervals. Turnovers were calculated from GC chromatographic analyses of the oxidation products.

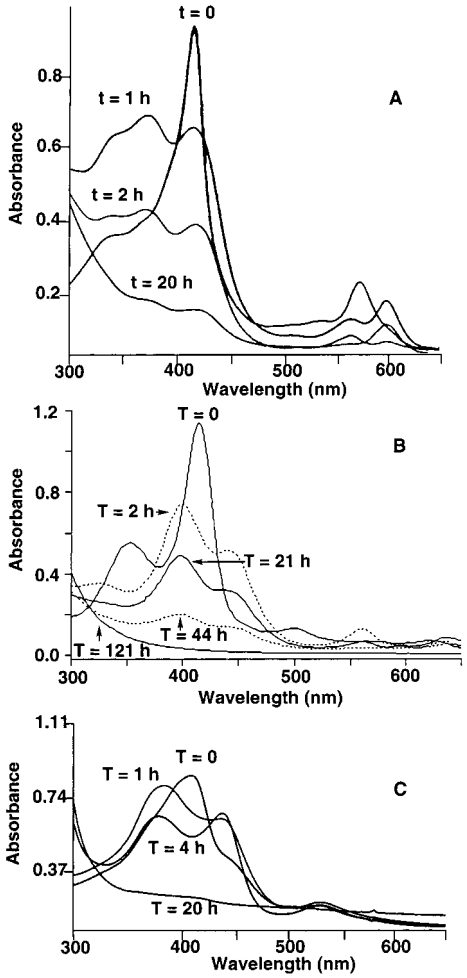

Figure 6. Time-dependent electronic absorption spectra of PFe-catalyzed isobutane oxidation reactions carried out in autoclave reactors when (A) $(C_3F_7)_4PFe-(py)_2$, (B) $(C_6F_5)_4PFe-Cl$, and (C) $Br_8(C_6F_5)_4$-PFe−Cl are utilized as catalyst precursors. Note the steady disappearance of benzene-soluble PFe complexes throughout the course of catalysis. Reactor conditions: $T = 80$ °C, [PFe] = 0.25 mM, $P_{O_2} = 8$ bar, [isobutane] = 22.8 mM (see the Experimental Section for further details). Optical spectra displayed were recorded at ambient temperature and pressure.

point in time at which electronic spectral analysis of the reaction medium indicated complete bleaching of all absorbances in the visible region, showing that the ultimate porphyrin-derived decomposition products are catalytically inactive.

While NMR and autoclave experiments show that the relative stabilities of the ferrous oxidation state in these macrocycle environments are surprisingly similar, there is no direct correlation between macrocycle stability under catalytic conditions and the thermodynamic stability of the ferrous oxidation state [($E_{1/2}$[$Fe^{II/III}$] (benzonitrile, 1.0 M pyridine) vs SCE: $Br_8(C_6F_5)_4$-PFe−$(py)_2$, 780 mV; $(C_3F_7)_4PFe-(py)_2$, 540 mV; $(C_6F_5)_4PFe-(py)_2$), 370 mV].[56] This suggests that a common catalyst deactivation mechanism may be operative, and implicates a role for radicals formed during the catalytic oxidation reaction (vide infra) in Fe−N, C−N, and/or C−C bond cleavage events.

It is likely that the enhanced reactivity reported previously for isobutane oxidation conditions utilizing $Br_8(C_6F_5)_4PFe$-based catalysts arises from two factors: (i) the high concentration of PFe−OH initially present in the reactions, which correlates with the observation that reactions utilizing this catalyst exhibit a burst of substrate turnovers in the first few minutes of reaction (Figure 5), and (ii) the fact that multiple ^{19}F signals are observed just after initiation of a $Br_8(C_6F_5)_4F$**e**-catalyzed reaction (Supporting Information). This latter point indicates that significant degradation of the highly halogenated macrocycle occurs just after catalysis commences, which raises the possibility that these (porphinato)iron decomposition products may also serve as initiators of isobutane autoxidation. Again, it is important to note that the overall activity of this catalyst with respect to the total turnovers of isobutane determined at the exhaustive limit of the oxidation reaction are similar to those observed for $(C_3F_7)_4PFe$- and **(**$C_6F_5)_4PFe$-catalyzed processes (Table 1), indicating that the concentration of active $Br_8(C_6F_5)_4PFe$-based catalysts must diminish rapidly with respect to time.

Axial Ligand and Solvent Effects on Catalyst Activity and Stability. Axial ligand electronic properties play a key role in the activation of dioxygen in heme-containing enzymes.[1] It has been demonstrated for synthetic metalloporphyrin catalysts, particularly for those systems which utilize O atom donors to generate reactive compound I analogues $P^{\bullet+}Fe{=}O-(L)$, that the nature of the metal axial ligand L influences both catalyst reactivity and stability; for instance, the addition of imidazole to a solution containing a PFe−Cl complex and excess organic peroxyacid, generates a PFe catalyst capable of epoxidizing olefins, while the high-valent PFe species generated in the imidazole-free solution are unreactive with respect to unsaturated hydrocarbons.[7] Likewise, for metalloporphyrin-catalyzed oxidations that consume oxidizing equivalents derived from dioxygen, Ellis and Lyons have reported that the introduction of azides as axial ligands for metalloporphyrin-catalyzed alkane oxidation results in augmented catalytic activity.[43,68]

The temperature-dependent ^{19}F and ^1H NMR studies (Figure 2; Supporting Information) evince reversible axial ligand dissociation for these $PFe-L_2$ systems, and demonstrate that the 3-F-py axial ligand resonance broadens due to exchange with increasing temperature. The effect of exogenous pyridine upon the catalytic isobutane oxidation reaction was probed in both autoclave and NMR reaction vessels. As seen in entries 1, 6, and 7 of Table 1A, no significant differences in catalyst reactivity or stability are observed for oxidation reactions in which autoclaves were charged with $(C_3F_7)_4PFe-Cl$ and $[(C_3F_7)_4PFe]_2O$ species relative to those in which $(C_3F_7)_4PFe-(py)_2$ served as the catalyst precursor. While the rate at which $PFe-(3\text{-F-py})_2$ complexes are converted to PFe^{III} species

(68) Lyons, J. E.; Ellis P. E., Jr.; Shaikh, S. N. *Inorg. Chim. Acta* **1998**, *270*, 162−168.

decreases with increasing exogenous 3-F-py concentrations (^{19}F NMR and autoclave reactor data not shown), once complete conversion of the PFe−L_2 precursor to the ferric porphyrin complex has taken place, a normal induction period is observed; both time-dependent electronic absorption and ^{19}F NMR reaction profiles are essentially identical to those obtained for the analogous reaction carried out in the absence of added axial ligand. These results reveal that enhanced stability for the ferrous oxidation state may be temporarily achieved by the addition of exogenous axial ligand, since hexacoordination precludes reactivity with dioxygen; augmented concentrations of 3-F-py, however, do not play a significant role in catalytic activity, product distribution, or ultimate catalyst lifetime.

Five different solvent systems were utilized for the PFe-catalyzed isobutane oxidation reactions: benzene, perfluoromethylcyclohexane (C_7F_{14}), 9:1 C_7F_{14}/benzene, 20:1 benzene/H_2O, and 20:1 benzene/(1 M aqueous NaOH). The PFe catalyst precursors and isobutane are highly soluble in both benzene and C_7F_{14}; while the major oxidation products are very soluble in benzene, their solubility is limited in C_7F_{14}. In general, little difference can be noted in these reactions as a function of solvent. Entries 3, 4, and 5 in Table 1A, however, relate the relative turnover numbers, product distribution, and selectivity for isobutane oxidation using a $(C_3F_7)_4$PFe−(3-F-py)$_2$ catalyst precursor in benzene, C_7F_{14}, and a 9:1 C_7F_4/benzene mixture; these results show that although the overall turnover numbers and conversion (%) do not vary significantly as a function of time in these reactions, the relative selectivity for *tert*-butyl alcohol over *tert*-butyl peroxide is enhanced in the oxidation reactions carried out with C_7F_{14} solvent. Similarly, entries 2 and 3 of Table 1B seem to show that added H_2O enhances the selectivity of *tert*-butyl alcohol over *tert*-butyl peroxide. While the data set is too limited to make broad conclusions regarding the role played by solvent in determining the distribution of oxidized hydrocarbons, the increased activity observed in catalytic hydrocarbon oxidations carried out with added water may derive from shifting the equilibrium described in Scheme 4 (equilibrium v, vide infra) toward PFe−OH. The lower level of *tert*-butyl peroxide (and the corresponding higher level of acetone) obtained for catalytic oxidations carried out in the presence of water likely correlates with enhanced rates of *tert*-butyl peroxide decomposition in this medium.

Role of Water in PFe-Catalyzed Isobutane Oxidation. High-Pressure ^{17}O NMR Spectroscopic Studies. Spectroscopic evidence (vide supra) shows that PFe−OH is present under catalytic conditions; production of this species would not be possible without a proton or hydroxide source. Because water would need only be present at levels approaching that of the catalyst concentration to be implicated in PFe−OH production, it is likely that sufficient moisture to do so would be present in the solvents and apparatus used for these reactions. (Except for entry 2 of Table 1A, no special care was taken to rigorously dry the solvents or reaction vessels used in this study.) To better understand the role played by water in PFe-catalyzed isobutane oxidations, small amounts of 20% enriched $^{17}OH_2$ were added to either benzene-d_6 solutions of $[(C_3F_7)_4PFe]_2O$ or a $[(C_6F_5)_4PFe]_2O$/$(C_6F_5)_4$PFe−OH equilibrium mixture under argon. Immediately, ^{17}O NMR reveals broadening of the free water signal relative to that observed for an $^{17}OH_2$ standard in benzene-d_6 (data not shown), suggesting either $^{17}OH_2$ association/dissociation is occurring with the PFe species present in solution on the time scale of the NMR experiment, or a chemical exchange process (eq 2) is taking place. Consistent with experiments

$$[PFe^{III}]_2O + {}^{17}OH_2 \rightleftharpoons \{Fe^{III}-OH + PFe^{III}-{}^{17}OH \quad (2)$$

carried out in aqueous systems,[69] ^{17}O NMR experiments executed with an independently synthesized sample of $(C_6F_5)_4$PFe−^{17}OH verify that the exchange process of eq 2 is facile in benzene. Interestingly, incorporation of the ^{17}O label into the oxidation products is observed when catalytic isobutane oxidation reactions are carried out in the presence of $^{17}OH_2$ (Table 2).

An alternating sequence of ^{17}O NMR and ^{19}F NMR spectra were repetitively recorded in which 5 μL of 20% enriched $^{17}OH_2$ was added to a 5 μM benzene solution of the PFe^{II} catalyst precursor prior to the sapphire NMR tube being charged with isobutane and unlabeled dioxygen under conditions identical to those described previously (Figure 7). As described above, following NMR tube pressurization with isobutane and dioxygen, ^{19}F NMR spectroscopy reveals the complete and irreversible formation of PFe^{III} species from the PFe^{II}-L_2 precursor, while ^{17}O NMR initially shows only one signal corresponding to the labeled water present in benzene-d_6 (Figure 7, spectrum B). At the point where new ^{17}O signals corresponding to hydrocarbon oxidation products are produced (spectrum F), a change in the nature of porphyrinic species present in solution is concomitantly observed (Figure 7, spectra E−G). The three major ^{17}O NMR signals in spectra F and H of Figure 7 correspond to acetone, *tert*-butyl peroxide, and *tert*-butyl alcohol; the integrated, relative intensities of the ^{17}O NMR peaks are consistent with those observed previously for analogous experiments in which ^{13}C NMR spectroscopy was used to monitor the relative amounts of isobutane oxidation products. The fact that ^{17}O signals are observed in the oxidation products highlights the direct involvement of water in the PFe-catalyzed oxidation of isobutane.

Two control experiments were performed to determine whether any ^{17}O oxygen incorporation into the hydrocarbon oxidation products occurs following the PFe-dependent catalytic reaction. Sapphire NMR tubes were charged with a benzene-d_6 solution of $(C_6F_5)_4$PFe−(3-F-py)$_2$, ^{17}O-labeled water, and either *tert*-butyl alcohol or *tert*-butyl peroxide (Table 2). The tubes were heated for a prolonged period (t = 2 days at 80 °C) and the organic products monitored by GC and ^{17}O NMR spectroscopy. As seen in Table 2, the experiment involving *tert*-butyl alcohol produced no other oxidized hydrocarbons; moreover, no ^{17}O incorporation into this alkanol was observed. However, when the tube was charged with *tert*-butyl peroxide under these conditions, acetone was generated with the incorporated ^{17}O label.[70] Thus, on the basis of these control experiments, we conclude that both *tert*-butyl alcohol and *tert*-butyl peroxide do not undergo ^{17}O exchange after their production in the isobutane oxidation, and this exchange must take place prior to their formation. Acetone, however, does exchange with water after its formation, and is produced in significant quantity through the decomposition of *tert*-butyl peroxide under the conditions of catalytic isobutane oxidation.

Role of Hydroperoxides in PFe-Catalyzed Isobutane Oxidation. *tert*-Butyl Hydroperoxide Decomposition Experiments. The catalytic decomposition of hydroperoxides by halogenated PFe complexes has been previously studied.[41−43] The major oxidation products reported in this reaction, namely,

(69) Ostrich, I. J.; Liu, G.; Dodgen, H. W.; Hunt, J. P. *Inorg. Chem.* **1980**, *19*, 619−621.

(70) Interestingly, no isobutanol was produced in this reaction, implying that isobutane or *tert*-butyl hydroperoxide must be present to generate this species, since the acetone generated in this experiment assuredly derives from *tert*-butoxy radical.

Table 2. Role of Water in PFe-Catalyzed Isobutane Oxidation: Evidence for Oxygen Exchange from Water Prior to Product Formation[a]

substrate	major oxidation products (GC or ^{13}C NMR)	^{17}O-labeled oxidation products (^{17}O NMR)
isobutane (400 mg)	*tert*-butyl alcohol acetone *tert*-butyl peroxide	*tert*-butyl alcohol acetone *tert*-butyl peroxide
tert-butyl alcohol (control) (40 μL)	*tert*-butyl alcohol	none
tert-butyl peroxide (control) (40 μL)	acetone *tert*-butyl peroxide	acetone

[a] Experimental conditions: solvent = benzene-d_6; [$(C_3F_7)_4$PFe$-$(3-F-py)$_2$] = 1.0 mM; [$^{17}OH_2$] = 0.14 M (20% ^{17}O enrichment); [isobutane] $\approx$7 M; O_2 pressure = $\sim$160 psi; T = 80 °C; reaction time = 2 days.

tert-butyl alcohol, acetone, and *tert*-butyl peroxide, are produced in proportions similar to those observed in PFe-catalyzed isobutane oxidations in which the oxidizing equivalents are derived from dioxygen; thus, the decomposition of such peroxides has been surmised to be important in the alkane oxidation reaction mechanism.[46,47,71] We have augmented this earlier work by utilizing in situ electronic absorption and ^{19}F NMR spectroscopic methods to probe the importance of this process in the PFe-catalyzed isobutane oxidation reaction and monitor the spectral changes that PFe complexes undergo during hydroperoxide decomposition.

Figure 8 shows the time-dependent electronic absorption spectral changes that occur for the $(C_3F_7)_4$P-, $(C_6F_5)_4$P-, and $Br_8(C_6F_5)_4$P-based iron catalyst systems in the presence of a 3000-fold molar excess of *tert*-butyl hydroperoxide. Isosbestic behavior was observed for the $Br_8(C_6F_5)_4$PFe-catalyzed reactions over a 1 h time period, highlighting the clean conversion of the ferrous porphyrin species to a single PFe^{III} complex (Figure 8A). In contrast, nonisosbestic behavior was observed in the analogous experiment utilizing the $(C_6F_5)_4$PFe catalyst (Figure 8B); interestingly, subsequent absorption spectra taken after the initial oxidation of $(C_3F_7)_4$PFe (Figure 8C) show little change with respect to the electronic absorption spectrum recorded at t = 10 min, indicating that these species may be a preferable peroxide decomposition catalyst due to its superior stability under these conditions. Note that, at 25 °C, no catalyst destruction is observed in the electronic absorption spectra, suggesting that the processes involved in PFe decomposition at 80 °C under oxidative conditions are slow at this temperature.

Significant macrocycle destruction, however, is observed in the electronic absorption spectra of these complexes recorded over longer time periods ($\sim$48 h) when large excesses of *tert*-butyl hydroperoxide are present; Figure 9 highlights such a set of data obtained when $(C_3F_7)_4$PFe$-$(3-F-py)$_2$ is used as the catalyst precursor. Time-dependent ^{19}F NMR spectra obtained for analogous *tert*-butyl hydroperoxide decomposition reactions in which $(C_3F_7)_4$PFe$-$(3-F-py)$_2$ and $(C_6F_5)_4$PFe$-$(3-F-py)$_2$ were utilized as catalyst precursors corroborate these results (Supporting Information); furthermore, these experiments (T = $-$70 to $-$20 °C) show the rapid conversion of these complexes to intermediates which were not observed during the in situ oxidation experiments and that, prior to the onset of the catalyst degradation, a single high-spin PFe^{III} species is present. It is interesting to note that, for $(C_6F_5)_4$PFe-catalyzed *tert*-butyl hydroperoxide decomposition reactions, there is no indication of the presence of [$(C_6F_5)_4$PFe]$_2$O by ^{19}F NMR or optical absorption spectroscopy, which contrasts the results reported above for the isobutane oxidation experiments (Figure 4).[51]

The potential role played by *tert*-butyl hydroperoxide in a PFe-catalyzed isobutane oxidation reaction was examined using in situ ^{19}F and ^{13}C NMR methods for a catalytic reaction employing a $(C_3F_7)_4$PFe$-$(3-F-py)$_2$ catalyst precursor; for these reactions, the NMR tube was charged with the PFe$-$(3-F-py)$_2$ complex, benzene-d_6, and 1000 equiv of *tert*-butyl hydroperoxide prior to pressurization with isobutane and dioxygen (Figure 10). Consistent with the data of Figure 3C, [$(C_3F_7)_4$PFe]$_2$O is the dominant PFe species present 30 min after the isobutane oxidation reaction has initiated (Figure 10B). It is noteworthy that if an induction period is taking place for this reaction, it must be less than the 2 h time period required for the acquisition of the spectrum of Figure 10B, since significant quantities of organic products were detected in a subsequently acquired ^{13}C NMR spectrum (data not shown). The induction periods for $(C_3F_7)_4$PFe-catalyzed reactions carried out under identical conditions without added hydroperoxide are minimally 8 h in duration. These data suggest that *tert*-butyl hydroperoxide serves to initiate the isobutane oxidation reaction. After 2 days at 80 °C, the spectrum in Figure 10C is evident. No further time-dependent spectral changes were observed due to the fact that all of the oxygen within the sapphire NMR tube was completely consumed at this point in time.

Summary and Conclusions

A variety of mechanisms have been proposed for PFe-catalyzed alkane oxidations that utilize dioxygen as the stoichiometric oxidant. Initially, it was hypothesized that the electron-deficient PFe species entered into a catalytic cycle which involves a high-valent PFe^{IV}=O intermediate.[40−45,65] Labinger and Gray proposed recently that an autoxidation reaction pathway likely dominated the kinetics; the primary role of the metalloporphyrin involved decomposing the hydroperoxides produced during the autoxidation pathway.[48−50] While the observed ratios of organic products produced in catalytic isobutane oxidation reactions did not coincide with that predicted by a theoretical model for such an autoxidation,[49] it was emphasized that if a P_{450}-type mechanism involving reactive PFe^{IV}=O species were to dominate, the selectivity toward *tert*-butyl alcohol would have been much higher than what is typically observed for these reactions.

Clearly, the mechanism by which the stoichiometric conversion of low-spin PFe$-L_2$ precursors to high-spin PFe^{III} species is accomplished at 80 °C in the presence of O_2 and isobutane provides additional information regarding the PFe oxidation states potentially important for catalysis; Scheme 3 shows three established pathways by which PFe^{III} species can be produced stoichiometrically from a PFe^{II} precursor. Routes that generate PFe^{III} requiring the production of superoxide by either a S_N1 or S_N2 process (pathway A) are not consistent with the observation of induction periods in both the NMR tube and autoclave experiments, as both these processes would produce peroxide; addition of even trace amounts of peroxide to either an autoclave or sapphire NMR tube isobutane oxidation reaction results in instantaneous termination of the induction period and the formation of organic products. Likewise, a water-assisted metal$-$superoxo decomposition (pathway B) produces the hydroperoxyl radical, an established radical chain autoxidation initiator. Control experiments rule out the generation of PFe^{III} species from trace peroxide impurities present in either the solvent or isobutane gas (pathway C) since (i) PFe^{III} species are stoichiometrically produced from the PFe$-L_2$ precursors

(71) Lyons, J. E.; Ellis, P. E., Jr. U.S. Patent 5345008 A, 1994.

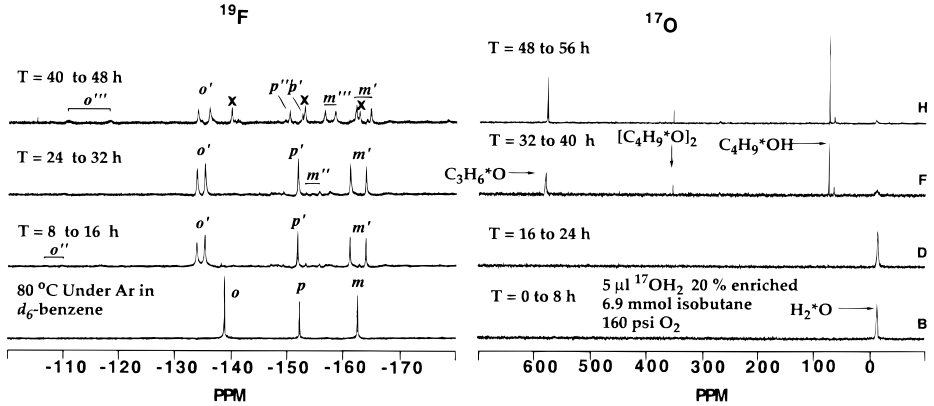

Figure 7. An alternating sequence of consecutively acquired ^{19}F and ^{17}O NMR spectra for a PFe-catalyzed isobutane oxidation reaction carried out at 80 °C in benzene-d_6 in which $(C_6F_5)_4PFe-(py)_2$ is used as the catalyst precursor. (A) ^{19}F NMR spectrum of $(C_6F_5)_4PFe-L_2$ at 80 °C under Ar. Spectra B−H that follow were taken during the time interval specified after the addition of labeled water, isobutane, and oxygen to the NMR tube. Prime notation represents the ^{19}F signals corresponding to $[(C_6F_5)_4PFe]_2O$, double prime notation represents resonances observed for $(C_6F_5)_4PFe-OH$, and triple prime notation denotes resonances that are tentatively ascribed to a $(C_6F_5)_4PFe-(O$-*tert*-butyl) complex. Resonances labeled with X are presently unassigned. All ^{17}O NMR spectra recorded at time intervals after spectrum F show the same relative intensities of the ^{17}O products; ^{19}F NMR spectra taken after spectrum F evince a steady decrease in concentration of benzene-soluble PFe species.

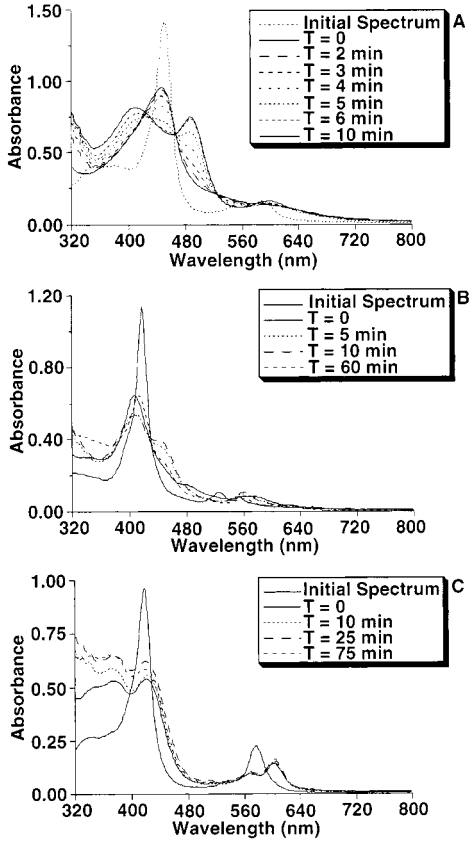

Figure 8. In situ time-dependent electronic absorption spectra of *tert*-butyl hydroperoxide decomposition reactions in benzene solvent in which (A) $Br_8(C_6F_5)_4PFe-(py)_2$, (B) $(C_6F_5)_4PFe-(py)_2$, and (C) $(C_3F_7)_4PFe-(py)_2$ were utilized as catalyst precursors. The trace labeled "initial spectrum" corresponds to the isolated ferrous porphyrin species in benzene under Ar; subsequent electronic absorption spectra taken at the labeled time intervals record the time-dependent optical changes that occur once a 3000-fold molar excess of *tert*-butyl hydroperoxide has been added. All spectra were taken at 26 °C. Experimental conditions: [PFe] = 10^{-5} M; [*tert*-butyl hydroperoxide] = 3×10^{-2} M.

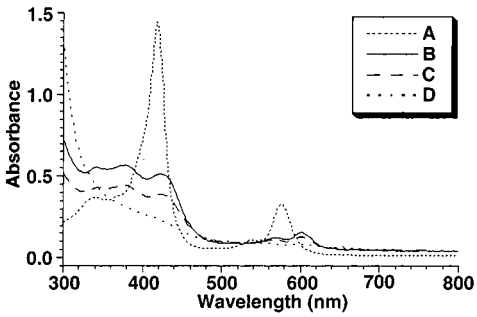

Figure 9. In situ time-dependent electronic absorption spectra recorded over long time intervals that chronicle a *tert*-butyl hydroperoxide decomposition reaction in which $(C_3F_7)_4PFe-(py)_2$ was utilized as a catalyst precursor. (A) $(C_3F_7)_4PFe-(py)_2$ under Ar. (B) $(C_3F_7)_4PFe-(py)_2$-derived species observed at $t = 5$ min following the addition of a 1000-fold molar excess of *tert*-butyl hydroperoxide. (C) $(C_3F_7)_4PFe-(py)_2$-derived species observed 12 h following the initial addition of *tert*-butyl peroxide. No further changes in the optical spectrum were apparent over an additional 1 h time period; at this point, an additional 2000 equiv of *tert*-butyl peroxide was added. (D) Optical spectra recorded 36 h after spectrum C.

in the *absence* of isobutane under O_2, (ii) ferrous $PFe-L_2$ complexes are completely converted to PFe^{III} species under dioxygen pressure even when the $PFe-L_2$ concentration is as high as 0.1 M (any peroxide or hydroperoxide impurity present at such a level would have been detectable by ^1H or ^{13}C NMR spectroscopy in the absence of catalyst, which was not the case), and (iii) reducing the concentration of the $PFe-L_2$ precursor to 1 μM shows only the production of PFe^{III} species in optically monitored oxidation experiments (oxidation products are observed only after the system is charged with isobutane and dioxygen, following the intermediacy of a normal induction period). If peroxide impurities exceeded this concentration level, one would expect to see reaction initiation and immediate observation of isobutane oxidation products upon addition of isobutane and dioxygen, which is not the case.

Given these facts, and the previously presented experimental evidence, we propose Scheme 4 as the most plausible mechanism by which PFe^{III} species are produced from these $PFe^{II}-L_2$ precursors. This scheme is based on a fourth, and extremely well-precedented, mechanism[72−74] that involves a transient PFe^{IV}═O species in the O_2-mediated ferrous-to-ferric porphyrin

(72) Chin, D.-H.; La Mar, G. N.; Balch, A. L. *J. Am. Chem. Soc.* **1980**, *102*, 4344−4350.
(73) Balch, A. L.; Renner, M. W. *Inorg. Chem.* **1986**, *25*, 303−307.
(74) Arasasingham, R. D.; Balch, A. L.; Cornman, C. R.; Latos-Grazynski, L. *J. Am. Chem. Soc.* **1989**, *111*, 4357−4363.

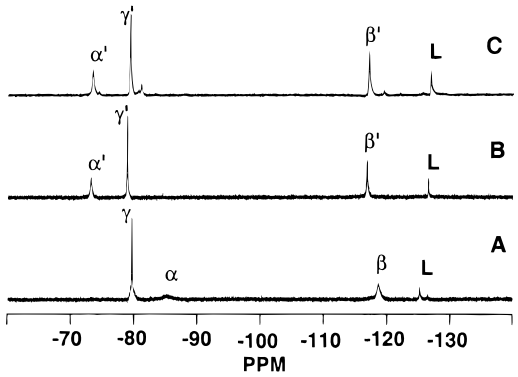

Figure 10. In situ ^{19}F NMR spectra that examine a PFe-catalyzed isobutane oxidation reaction in which a $(C_3F_7)_4$PFe−(3-F-py)$_2$ catalyst precursor was utilized in the presence of 1000 equiv of *tert*-butyl hydroperoxide. (A) The PFe−L_2 complex at 26 °C under Ar in benzene-d_6. (B) ^{19}F NMR spectrum taken at 80 °C 30 min after O_2/isobutane/*tert*-butyl hydroperoxide addition. Alcohol production is observed in the ^{13}C NMR at this time (spectrum not shown). (C) ^{19}F NMR spectrum obtained at 80 °C after data were acquired over the 48−50 h time following O_2/isobutane/*tert*-butyl hydroperoxide addition; at this point in time, the dioxygen contained in the NMR tube was completely consumed. The resonance labeling scheme is identical to that described in Figure 3.

conversion. Although PFe^{IV}═O species have been isolated and characterized,[75] because the species in brackets are not spectroscopically detected under our experimental conditions, this route for the PFe^{II}-to-PFe^{III} conversion can only be considered a postulate. We emphasize, however, that the most attractive feature of this proposal is the fact that it produces no species (HOOH, O_2^-) that either are known to directly initiate or can be converted to species that directly initiate isobutane autoxidation in the presence of PFe complexes.[49] It is important to note that all other commonly invoked mechanisms for an O_2-mediated PFe^{II}-to-PFe^{III} conversion fail this crucial test. Processes i−v of Scheme 4 must be rapid, since PFe−OH and/or $(PFe)_2O$ complexes are observed immediately upon pressurization of either a sapphire NMR tube or an autoclave reactor containing a PFe^{II}−L_2 solution with dioxygen (t < 15 min. If the mechanism of Scheme 4 is operative, the transiently generated PFe^{IV}═O species must either react with hydrocarbon substrates on a time scale that is long with respect to that for reaction iv (Scheme 4) or not be thermodynamically competent to promote alkane hydroxylation. This latter hypothesis is consistent with thermodynamic data compiled by Sawyer which indicate that the Fe^{IV}═O + H$^\bullet$ → Fe−OH bond formation energy ($-\Delta G_{BF}$) compares unfavorably with the dissociative bond energy ($-\Delta H_{BDE}$) required for isobutane C−H bond homolysis.[76−78] We thus propose that isobutane oxidation is initiated by a mechanism that involves the thermodynamically unfavorable homolysis of the PFe−OH bond. This proposal is attractive for four reasons: (i) It is consistent with the long and often widely variable induction periods. (ii) It accounts for the presence of the small quantities of the primary alkane oxidation product, 2-methyl-1-propanol, observed in these reactions, because H-atom abstraction processes involving hydroxyl radicals and primary alkanes are thermodynamically favored in benzene.[79] (iii) Any HO$^\bullet$ that escapes the [PFe^{II}−OH] cage would initiate an autoxidation mechanism. (iv) The lengths of the induction periods that are observed for these reactions correlate with the magnitudes of previously reported PFe−OH bond dissociation energies.[80]

Once H atom abstraction from isobutane occurs, the organic radical will react with dioxygen and initiate an autoxidation radical chain process; this modified Haber−Weiss cycle is shown in Scheme 5. While some of the details of Scheme 5 are speculative in nature, note that the propagation step described in Scheme 5A produces the *tert*-butyl hydroperoxyl radical. Oxidized organic products are created through the PFe-catalyzed decomposition of the hydroperoxide (Scheme 5B,C); extensive low-temperature spectroscopic data obtained by Balch establish precedent for the mechanistic role ascribed to PFe^{III}-bound *tert*-butyl hydroperoxo compounds.[74,81−84] The ^{17}O NMR experiments provide insight into the nature of the PFe-catalyzed hydroperoxide decomposition process; because the ^{17}O label is observed in all the major organic products produced in the reaction (*tert*-butyl alcohol, acetone, and *tert*-butyl peroxide), PFe−OH must play a major role in *tert*-butyl hydroperoxide decomposition as well as reaction initiation.

A number of reactions known to occur under Haber−Weiss conditions have been omitted from Scheme 5 for the sake of clarity. With respect to the ^{17}O-labeling experiments, a few of these such reactions are worth noting in brief. It is well-known that (porphinato)iron(III)−(alkyl peroxide) species (Scheme 5B), in addition to undergoing bond homolysis reactions that produce PFe(II) species and peroxyl radicals, decompose via both homolytic and heterolytic O−O bond cleavage processes.[7,37,85−87] Either homolytic or heterolytic cleavage enables facile incorporation of the ^{17}O label into the β-oxygen atom of the peroxyl group. Once this occurs, two pathways allow incorporation of the ^{17}O label into *tert*-butyl alcohol. As noted previously, the ^{17}O-labeling experiments were carried out in sapphire NMR tubes that utilized 8:1 isobutane/dioxygen (see the Experimental Section); these reactions were run until catalysis ceased, and exhibited isobutane conversions that ranged from 5% to 10%. Because this corresponds to incorporation of 40−80% of the O_2 present in the NMR tubes into products, the fact that cycle

(75) Groves, J. T.; Gross, Z.; Stern, M. K. *Inorg. Chem.* **1994**, *33*, 5065−5072.
(76) Fe^{IV}═O + H$^\bullet$ → Fe(III)−OH ($-\Delta G_{BF}$ = 78 kcal/mol); $(CH_3)_3CH$ → $(CH_3)_3C^\bullet$ + H$^\bullet$ ($-\Delta H_{BDE}$ = 93 kcal/mol).
(77) Sawyer, D. T. *J. Phys. Chem.* **1989**, *93*, 7977−7978.
(78) *The Activation of Dioxygen and Homogeneous Catalytic Oxidation*; Barton, D. H. R., Martel, A. E., Sawyer, D. T., Eds.; Plenum Press: New York, 1993; pp 1−7.
(79) $H_3CCH_2CH_3$ → $H_3CCH_2CH_2^\bullet$ + H$^\bullet$ ($-\Delta H_{BDE}$ = 100 kcal/mol); H_2O → HO$^\bullet$ + H$^\bullet$ ($-\Delta H_{BDE}$ = 111 kcal/mol).
(80) Assuming that a typical induction period of 6 h correlates directly with $^\bullet$OH escape from a [PFe^{II}$^\bullet$OH] cage, and that the cage recombination reaction to produce PFe−OH occurs at diffusion-controlled rates (10^9 M^{-1} s^{-1}), gives an equilibrium constant $K = 4.63 \times 10^{-14}$ M^{-1} at 80 °C. Provided that $\Delta S°$ for this reaction does not deviate appreciably from 23 eu, a standard value for bond homolysis reactions (see for example: (a) *Handbook of Chemistry and Physics*, 71st ed.; CRC Press: Boca Raton, FL, 1990; pp D51−D95. (b) Woska, D. C.; Xie, Z. D.; Gridnev, A. A.; Ittel, S. D.; Fryd, M.; Wayland, B. B. *J. Am. Chem. Soc.* **1996**, *118*, 9102−9109) allows an estimation of ΔH_{BDE} = 30 kcal mol^{-1}. This value lies intermediate in the range of ΔH_{BDE} values for PFe−OH complexes that have been measured to date (see: Richert, S. A.; Tsang, P. K. S.; Sawyer, D. T. *Inorg. Chem.* **1989**, *28*, 2471−2475. Tung, H. C.; Chooto, P.; Sawyer, D. T. *Langmuir* **1991**, *7*, 1635−1641).
(81) Arasasingham, R. D.; Balch, A. L.; Latos-Grazynski, L. *J. Am. Chem. Soc.* **1987**, *109*, 5846−5847.
(82) Arasasingham, R. D.; Balch, A. L.; Har, R. L.; Latos-Grazynski, L. *J. Am. Chem. Soc.* **1990**, *112*, 7566−7571.
(83) Balch, A. L. *Inorg. Chim. Acta* **1992**, *198*, 297−307.
(84) Balch, A. L.; Olmstead, M. M.; Safari, N.; St. Claire, T. N. *Inorg. Chem.* **1994**, *33*, 2815−2822.
(85) He, G.-X.; Bruice, T. C. *J. Am. Chem. Soc.* **1991**, *113*, 2747−2753.
(86) Traylor, T. G.; Tsuchiya, S.; Byun, Y.-S.; Kim, C. *J. Am. Chem. Soc.* **1993**, *115*, 2775−2781.
(87) Traylor, T. G.; Kim, C.; Richards, J. L.; Xu, F.; Perrin, C. L. *J. Am. Chem. Soc.* **1995**, *117*, 3468−3474.
(88) Lyons, J. E.; Ellis, P. E., Jr.; Myers, H. K., Jr. *J. Catal.* **1995**, *155*, 59−73.

Scheme 3. Mechanisms by Which PFe^{III} Species Can Be Generated from PFe^{II} Precursors under Oxidative Conditions: (A) Generation of Superoxide by S_N1 or S_N2 Pathways; (B) H_2O-Assisted Metal Superoxo Decomposition; (C) Direct Oxidation via Hydroperoxide Impurities Present in Isobutane and/or Solvent

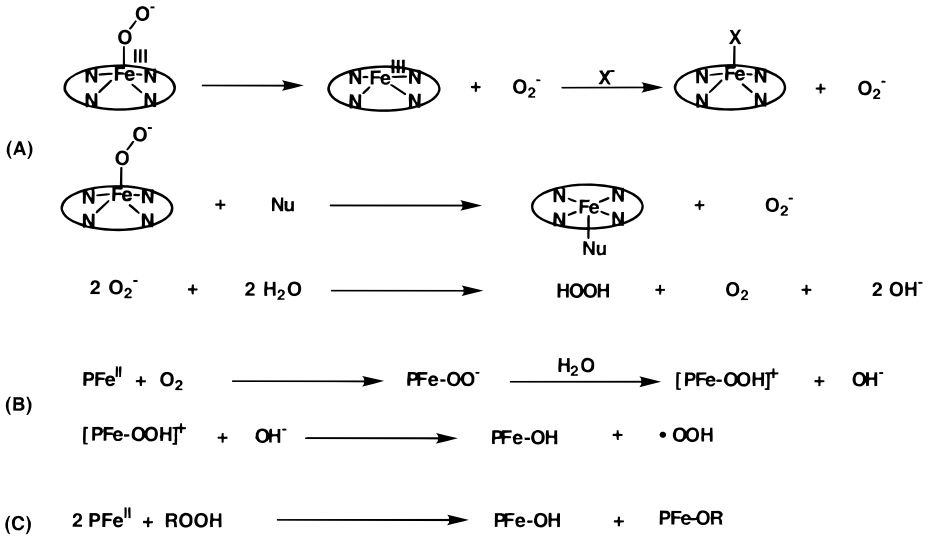

Scheme 4. Proposed Initiation Mechanism for PFe-Catalyzed Isobutane Oxidation

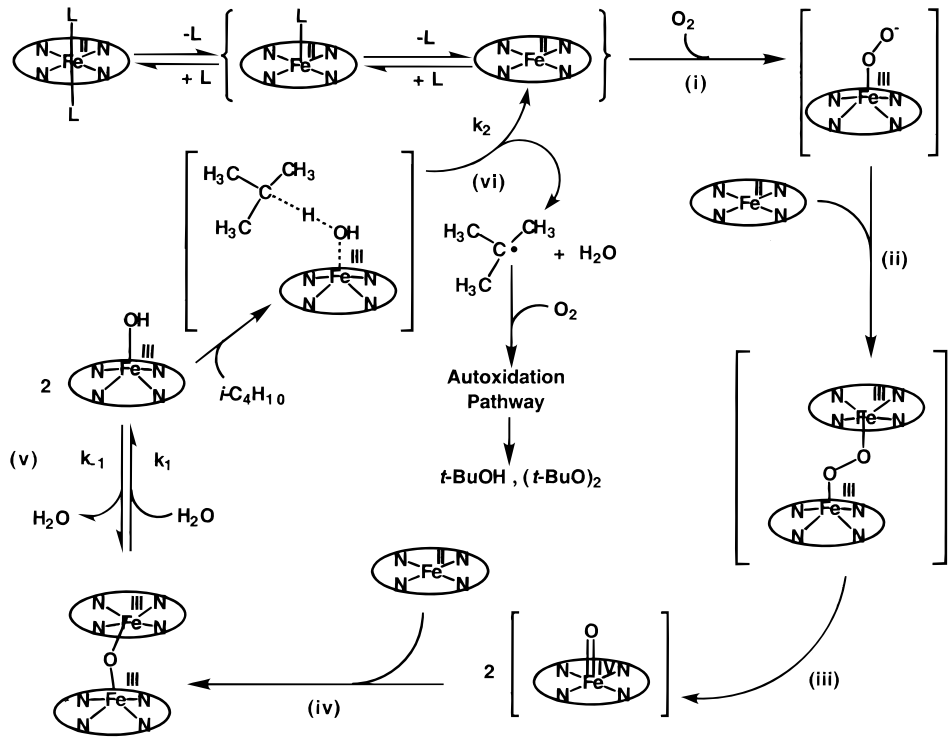

C of Scheme 5 produces labeled dioxygen enables ^{17}O to be introduced into the α-peroxyl position and hence into the *tert*-butyl alcohol, since labeled dioxygen would be free to reenter the catalytic cycle of Scheme 4A. Alternatively, the common Haber−Weiss reaction that produces *tert*-butyl peroxide via the reaction of *tert*-butyl radical and *tert*-butyl peroxyl radical provides a second route to ^{17}O-labeled *tert*-butyl alcohol (Scheme 5C). Because the majority of the ^{17}O label at the end of the catalytic reaction is incorporated into products, the PFe−OH-dependent process of Scheme 5B must be the focal point for peroxide decomposition.

A large body of work has been dedicated to the study of PFe-catalyzed alkane oxidation using dioxygen as the stoichiometric oxidant.[41−43,46−48,50,67,88−90] Although electron-deficient PFe complexes are competent to catalyze isobutane oxidation at moderate temperatures without the input of stoichiometric reductants, such simple catalysts are not stable under the autoxidation reaction conditions. While porphyrin ring halogenation leads to more robust epoxidation catalysts that utilize PFe^{III} complexes and an O atom donor to produce reactive compound I analogues ($P^{\bullet+}Fe^{IV}{=}O$),[9,91,92] PFe alkane hydroxylation catalysts that derive their oxidizing equivalents from O_2

(89) Ellis, P. E., Jr.; Lyons, J. E.; Shaikh, S. N. *Catal. Lett.* **1994**, *24*, 79−83.
(90) Lyons, J. E.; Ellis, P. E., Jr. *Appl. Catal., A* **1992**, *84*, L1-L6.
(91) Traylor, T. G.; Dunlap, B. E.; Miksztal, A. R. *Basic Life Sci.* **1988**, *49*, 509−512.
(92) Traylor, P. S.; Dolphin, D.; Traylor, T. G. *J. Chem. Soc., Chem. Commun.* **1984**, 279−280.

Scheme 5. Modified Haber−Weiss Radical Chain Mechanism for PFe-Catalyzed Alkane Oxidation and Hydroperoxide Decomposition

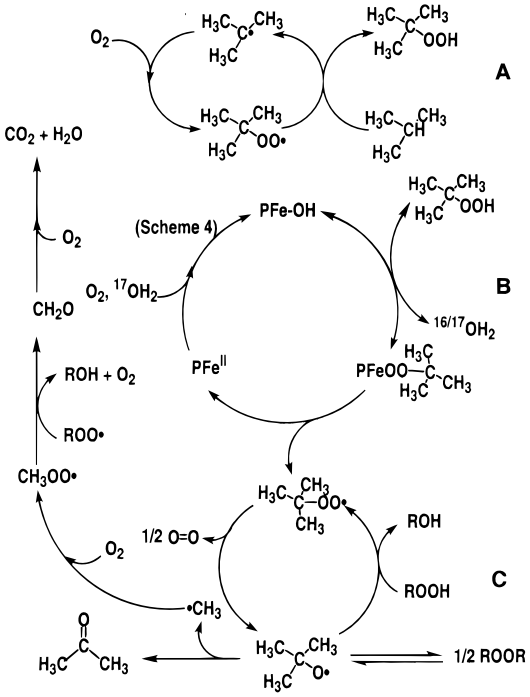

that are based on highly halogenated $Br_8(C_6F_5)_4PH_2$ ligand systems possess stabilities that are *diminished* relative to those of analogous catalysts that feature $(C_6F_5)_4PH_2$ and $(C_3F_7)_4PH_2$ ligand frameworks.

Last, with respect to the conversion of PFe^{II} to PFe^{III} within the context of an autoxidation mechanism, it has been proposed that peroxides play a key role in this process and that alkoxyl radicals and hydroxide anions are produced stoichiometrically each time a ferrous center is oxidized.[48] This study demonstrates that such a role for ROOH is unlikely due to its extremely low concentration under these experimental conditions and that O_2 is responsible for this conversion in the catalytic cycle (Scheme 5). Since hydroperoxides are not detected at any point in the catalytic reaction, their concentration must be lower than the detection limit of the NMR spectrometer. Assuming that hydroperoxide present at concentrations higher than 1/25 of that for the catalyst would be detectable, the upper limit for the hydroperoxide concentration is $\sim 10^{-3}$ mM. This value is at least 4 orders of magnitude smaller than the concentration of O_2 in benzene under these conditions, which is ∼10 mM at 353 K and 1 atm of O_2 pressure.[93,94]

This study highlights two roles for the PFe complexes in catalytic isobutane oxidation: that of the radical chain initiator and, consistent with work by Labinger and Gray,[48,50,67] the species responsible for the catalytic decomposition of organic peroxides. It is thus appropriate to consider the dual requirements of radical chain initiation and facile hydroperoxide decomposition, and whether a set of experimental conditions and catalysts can be elucidated that allows for control of •OH concentration and facile hydroperoxide decomposition, while protecting the catalyst from decomposition. Furthermore, with respect to catalyst design and the original proposal by Ellis and Lyons,[40−45,65] the development of a ligand framework that will allow a PFe^{IV}═O species to replicate the chemistry of the biological $P^{\bullet+}Fe^{IV}$═O paradigm, and direct the incorporation of both O atoms of O_2 into organic substrates while suppressing autoxidation radical chain processes, clearly remains a challenging problem in biomimetic chemistry.

Acknowledgment. M.J.T. thanks the Office of Naval Research (Grant N00014-98-1-0187) for their generous support of this work, and gratefully acknowledges the Searle Scholars Program (Chicago Community Trust), the Arnold and Mabel Beckman Foundation, and the National Science Foundation for Young Investigator Awards, as well as the Camille and Henry Dreyfus and Alfred P. Sloan Foundations for research fellowships. I.T.H. acknowledges the support of the Exxon Research and Engineering Co. for his work in the area of hydrocarbon activation. We thank James T. Fletcher for preparing several figures in this manuscript, acknowledge Raymond A. Cook, Kenneth A. Eriksen, and Jeffrey E. Bond for their invaluable experimental assistance, and express gratitude to Drs. Paul A. Stevens, Walter Weismann, István Pelcer, and David Woska for many stimulating discussions.

Supporting Information Available: Spectroscopic data that detail the temperature and axial ligand concentration dependences of NMR chemical shifts of these (porphinato)iron complexes, along with additional catalytic isobutane oxidation and *tert*-butyl hydroperoxide decomposition data. This material is available free of charge via the Internet at http://pubs.acs.org.

IC000284O

(93) Byrne, J. E.; Battino, R.; Danforth, W. F. *J. Chem. Thermodyn.* **1974**, *6*, 245−250.

(94) Bimolecular rate constants for dioxygen binding at five-coordinate PFe−(L) complexes typically range from 1×10^6 to 5×10^8 M^{-1} s^{-1} at ambient temperature (See: Momenteau, M.; Reed, C. A. *Chem. Rev.* **1994**, *94*, 659−698), with sterically unencumbered ferrous porphyrin complexes displaying an average bimolecular rate constant of $\sim 5 \times 10^7$ M^{-1} s^{-1}. Because the dioxygen concentration exceeds that of *tert*-butyl hydroperoxide by at least a factor of 10^4, for reoxidation of PFe(II) by *tert*-butyl hydroperoxide to compete with the dioxygen-mediated reaction, the bimolecular rate constant for this process would have to exceed that for a diffusion-controlled process by (at least) a factor of 1000.